An Exactly Fragment Additive Breakdown of

Polarization for Energy Decomposition Analysis

Based on the Self-Consistent Field for Molecular

Interactions.

Hengyuan Shen, Srimukh Prasad Veccham, and Martin Head-Gordon\*

Pitzer Center for Theoretical Chemistry, Department of Chemistry, University of

California, Berkeley, California 94720, USA

E-mail: mhg@cchem.berkeley.edu

Abstract

Energy decomposition analysis (EDA) is a useful method to unravel an intermolecular inter-

action energy into chemically meaningful components such as geometric distortion, frozen

interactions, polarization, and charge transfer. A further decomposition of the polarization

(POL) and charge transfer (CT) energy into fragment-wise contributions would be useful to

understand the significance of each fragment during these two processes. To complement the

existing exact pairwise decomposition of the CT term, this work describes formulation and

implementation of a non-perturbative polarization analysis that decomposes the POL energy

into an exactly fragment-wise additive sum based on the absolutely localized molecular or-

bital energy decomposition analysis (ALMO-EDA). These fragment-wise contributions can

be further decomposed into chemically intuitive molecular orbital pairs using complementary

occupied-virtual pairs (COVP) analysis. A very useful phase convention is established for

1

each COVP such that constructive interference of occupied and virtual corresponds to electron flow into that region, whilst destructive interference corresponds to electron outflow. A range of model problems are used to demonstrate that the polarization process is typically a collective behavior of the electrons that is quite different from the charge transfer process. This provides another reason in addition to their different distance-dependence on fragment separation for separating these two processes in EDA.

#### 1 Introduction

Quantum mechanically based electronic structure calculations of interaction energies are like numerical experiments: they can yield precise values for observable energy differences, but do not explain why those differences are small or large. To fill the gap, energy decomposition analysis (EDA) methods <sup>1-6</sup> aim to provide chemical insights about intermolecular interactions by breaking the interaction energies into physically meaningful terms such as electrostatics, dispersion interaction, Pauli repulsions, induced electron polarization and charge transfer. <sup>7-10</sup> These partitions provide a link between the quantum mechanical calculations and chemical interpretation by revealing the dominant contributions to intermolecular interactions, or, chemical bonds. Not only can one better understand the interacting system, but this can also facilitate rational materials design, by guiding modifications such as chemical substitutions to get desired functional outcomes. Though the EDA components are not uniquely defined, they can nevertheless be designed to satisfy suitable properties such as being basis function independent, demonstrating correct asymptotic behavior, and corresponding to Fermionic quantum mechanical energies. <sup>11</sup> These considerations are discussed in detail in a recent overview of EDA. <sup>6</sup>

The charge transfer (CT) term corresponds to the energy decrease of the interacting system due to inter-fragment electron delocalizations. When several fragments are placed close to each other, the electrons of one fragment can delocalize to other fragments to decrease the energy of the system.<sup>12</sup> This is a key step in the formation of chemical bonds with partial ionic character<sup>13</sup> and the dative (or donor-acceptor) contribution to non-bonded interactions.<sup>12,14</sup> By contrast, the polarization (POL) process describes charge rearrangements within each fragment in response to the local electric fields and filled orbital interactions associated with the presence of other fragments.<sup>11</sup> It is quite common to combine POL and CT within an EDA, as exemplified by the orbital rearrangment (ORB) term of the extended transition state<sup>1</sup> - natural orbitals for chemical valence (ETS-NOCV) approach,<sup>9</sup> or the localized MO (LMO)-EDA method.<sup>10</sup> The induction (IND) terms of symmetry-adapted perturbation theory (SAPT)<sup>15-17</sup> also naturally contain both POL and CT.

If one wishes to separate POL from CT, one quite natural approach is to apply a Hilbertspace constraint in which the orbitals of a given fragment can only mix with virtual orbitals associated with the same fragment. This selective mixing retains fragment block-diagonal structure of the molecular orbital (MO) coefficient matrix. 18-22 One example is using just the atomic orbitals (AOs) of each fragment to provide its virtuals. However, a problem with using the whole virtual spaces of fragments is its unsatisfactory behavior in large atomic orbital (AO) basis sets, where the fragment subspaces become linearly dependent. 11,12,23,24 This problem was solved by keeping only the fragment electric-field response functions (FERF)<sup>11</sup> in the virtual spaces, which eliminates the subspace linear dependence issue while maintaining the ability to describe fragments' orbital response to the external multi-poles. Either type of fragment-specific relaxation can be accommodated with the self-consistent field for intermolecular interactions (SCFMI) method  $^{18-22}$  or generalizations of SCF-MI.  $^{14}$  Within variational EDA, performed within either Hartree-Fock or Kohn-Sham density functional theory (DFT), SCFMI was first used in the block-localized wavefunction (BLW)  $EDA^{25-27}$ to separate POL and CT. The same approach is used in the absolutely localized MO EDA (ALMO-EDA), 8,28,29 where the ALMOs refer to the fragment localized orbitals.

There are also other methods that have been proposed to separate POL from CT. The pioneering Kitaura-Morokuma (KM) EDA<sup>7,30</sup> defined the polarized state as the product of

the polarized fragment wavefunctions. However, this does not correspond to a valid antisymmetric wavefunction, and thus violates Pauli's exclusion principle. The constrained density functional theory (CDFT) approach constructs the polarized state by minimizing the system energy while requiring the real-space population on a certain fragment to be a specified integer. <sup>31,32</sup> Within SAPT, there have been suggestions to manipulate the atomic or molecular basis sets to suppress excitations that are of charge transfer type, <sup>33,34</sup> or by regularizing the nuclear potential to suppress tunneling induced charge transfer. <sup>35,36</sup> CDFT has also been used within SAPT to separate POL and CT. <sup>12,24</sup> The natural energy decomposition analysis (NEDA) treats the polarization together with the electrostatic component as the potential energy contribution. <sup>37</sup> A variational scheme that has been recently developed is the valence bond EDA (VB-EDA) scheme, where the polarization component is described as orbital relaxations from monomers' orbitals to supermolecule's orbitals. <sup>38</sup>

With a well-defined separation of POL and CT, it is natural to further analyze these terms to characterize their separate contributions to intermolecular interactions. Within the ALMO-EDA, a perturbative CT analysis (CTA) was proposed<sup>39</sup> in terms of complementary occupied-virtual orbital pairs (COVPs). This analysis has proved quite useful, and, more recently, the perturbative restriction was removed leading to an exact COVP analysis for CT.<sup>40</sup> Alternatively, the ETS-NOCV scheme<sup>9</sup> is widely used to analyze the union of CT and POL, leading to the chemically insightful NOCVs and their contribution to ORB. It is also possible to use the NOCVs to connect any pair of states<sup>41</sup> and for CT, this yields results that are closely related to the non-perturbative ALMO-CTA.<sup>40</sup>

The purpose of this paper is to present a polarization analysis within the ALMO-EDA framework. The objective of this analysis is to decompose the polarization energy,  $\Delta E_{\rm POL}$ , exactly into a sum of contributions from each fragment, X, of a molecular complex or supersystem:

$$\Delta E_{\rm POL} = \sum_{x} \Delta E_{\rm POL}^{x} \tag{1}$$

The charge rearrangement associated with the polarization process can likewise be exactly

decomposed into a sum of fragment contributions:

$$\Delta Q_{\rm POL} = \sum_{x} \Delta Q_{\rm POL}^{x} \tag{2}$$

Of course polarization is a many-body process, <sup>42</sup> so the sum of one-body contributions from individual fragments is an effective description that allows a simple overall view of the coupled many-body POL process. The many-body expansion itself can be condensed into effective contributions in much the same way. <sup>43</sup>

The POL process connects a starting state, which corresponds to the frozen orbitals of each isolated fragment,  $^{44}$  to the final polarized state, in which the fragment orbitals relax in the presence of each other through SCFMI. The FRZ  $\rightarrow$  POL path mixes occupied (i) and virtual (a) orbitals on fragment x by a matrix with elements  $X_{ia}^x$ .  $\mathbf{X}^x$  contains the generators of the unitary transformation matrix connecting the end-points. There is no explicit mixing of orbitals on different fragments to ensure that CT is separated from POL: the many-body effects arise by coupling between degrees of freedom on different fragments to minimize the POL energy via SCF-MI. By singular value decomposing the fragment-blocked matrices  $\mathbf{X}^x$ , we obtain POL-specific complementary occupied virtual orbital pairs (COVPs) belonging to each fragment. These COVPs give the most compact possible description of the POL-induced energy lowering and charge rearrangments.

The remainder of the paper is organized as follows. The theory necessary to define the contributions discussed above is presented in Sec. 2. To explore the character of the POL process and illustrate the usefulness of our ALMO-PA, we then analyze a series of examples of increasing chemical complexity. First, we examine the toy model of a hydrogen atom in a uniform electric field, which is largely an analytical example. Then we consider the polarization of a helium atom by a lithium cation, as a function of inter-atomic distance. Followed by the above is the Ne-Ar<sup>+</sup> cluster at various inter-atomic distance. Two hydrogen bonded systems are then examined: water-chloride, and the water dimer. Finally the interaction

between a sodium cation and a polycyclic aromatic hydrocarbon radical is studied.

# 2 Theory

#### 2.1 Notation

In this section, we will introduce the notation used in the following derivations. We use Latin letters x, y, z, w, v to denote fragments, letters i, j, k, l, m, n to label occupied molecular orbitals, letters a, b to label virtual molecular orbitals, letters p, q, r, s to label general molecular orbitals, and Greek letters  $\alpha, \beta, \gamma$  to label atomic orbitals. We denote molecular orbitals as  $|\psi\rangle$  and atomic orbitals as  $|\omega\rangle$ . o and v are the total number of occupied and virtual MOs, while n and n are the total number of MOs and AOs. n0 denotes the number of fragments. The AO overlap matrix is defined as n0 as n1 and n2 are the occupied MO overlap matrix is defined as n3 and the occupied MO overlap matrix is defined as n4 and n5 and the occupied MO overlap matrix is defined as n5 and the occupied MO overlap matrix is defined as n5 and the occupied MO overlap matrix is defined as n5 and the occupied MO overlap matrix is defined as n6 and n7 are the total number of MOs and AOs. n8 and the occupied MO overlap matrix is defined as n6 and n7 are the total number of MOs and AOs. n8 and the occupied MO overlap matrix is defined as n6 and n8 are the total number of MOs and AOs. n9 and the occupied MO overlap matrix is defined as n6 and n8 are the total number of MOs and AOs. n9 and the occupied MO overlap matrix is defined as n8 and n9 are the total number of MOs and AOs. n9 are the total number of MOs and AOs. n9 are the total number of MOs and AOs. n9 are the total number of MOs and AOs. n9 are the total number of MOs and AOs. n9 are the total number of MOs and AOs. n9 are the total number of MOs and AOs. n9 are the total number of MOs and AOs. n9 are the total number of MOs and AOs. n9 are the total number of MOs and AOs. n9 are the total number of MOs and AOs. n9 are the total number of MOs and AOs. n9 are the total number of MOs and AOs. n9 are the total number of MOs and AOs. n9 are the total number of MOs and AOs. n9 ar

$$|\psi^{xr}\rangle = \sum_{us}^{n} (\sigma^{-1})_{ys,xr} |\psi_{ys}\rangle, \tag{3}$$

It can be easily shown that  $\langle \psi^{xr} | \psi_{ys} \rangle = \delta_{xy} \delta_{rs}$ . We used real orbitals in this paper, although the generalization to complex orbitals can be similarly derived.

## 2.2 Summary of results

This ALMO polarization analysis is able to naturally separate the energy transfer and electron rearrangements of the POL process into fragment-wise additive terms. This is achieved by connecting each fragment's density matrix from the FRZ state to the POL state with a unitary transformation  $\mathbf{U}^{(x)}$ , such that  $\mathbf{P}_{\text{POL}}^{(x)} = \mathbf{U}^{(x)}\mathbf{P}_{\text{FRZ}}^{(x)}\mathbf{U}^{(x)T}$  expressed in each fragment's

orthonormal MO basis. The unitary transformation is parameterized as

$$\mathbf{U}^{(x)} = \exp\left(\mathbf{X}_{\text{POL}}^{(x)}\right) = \exp\left(\begin{array}{cc} 0 & \left(\mathbf{X}_{\text{POL}}^{(x)}\right)_{ov} \\ -\left(\mathbf{X}_{\text{POL}}^{(x)}\right)_{ov}^{T} & 0 \end{array}\right),\tag{4}$$

where the rectangular matrix  $\mathbf{X}_{ov}^{(x)}$  is of dimension  $o \times v$ , which are the number of occupied and virtual orbitals of fragment x. The amount of charge transferred during polarization is defined as <sup>39</sup>

$$\Delta Q = \text{Tr} \left\{ \hat{P}_{POL} \right\} - \text{Tr} \left\{ \hat{P}_{POL} \hat{P}_{FRZ} \right\} = \text{Tr} \left\{ \hat{P}_{POL} \hat{Q}_{FRZ} \right\}, \tag{5}$$

where  $\hat{P}_{FRZ}$  and  $\hat{P}_{POL}$  are the density operators of the FRZ and POL states, while  $\hat{Q}_{FRZ}$  is the virtual space projector of the FRZ state. Through a parameterization of the energy and charge, we can decompose the charge transfer  $\Delta Q$  and the energy transfer  $\Delta E = E_{POL} - E_{FRZ}$  as

$$\Delta Q = \sum_{x} \text{Tr} \left\{ \hat{P}_{vo}^{\text{eff}(x)} \left( \hat{X}_{POL}^{(x)} \right)_{ov} \right\} = \sum_{x} \Delta Q^{(x)}$$
 (6)

$$\Delta E = \sum_{x} \text{Tr} \left\{ \hat{F}_{vo}^{\text{eff}(x)} \left( \hat{X}_{POL}^{(x)} \right)_{ov} \right\} = \sum_{x} \Delta E^{(x)}, \tag{7}$$

where  $\hat{P}_{vo}^{\text{eff}(x)}$  and  $\hat{F}_{vo}^{\text{eff}(x)}$  are the effective density operator and effective fock operator of each fragment, whose exact expressions will be shown later.

# 2.3 Non-perturbative energy transfer analysis

The total energy along a linear path between the frozen state ( $\lambda = 0$ ) and the polarized state ( $\lambda = 1$ ) can be parameterized as

$$E[\lambda] = E\left[\mathbf{X}^{(x)}(\lambda), \mathbf{X}^{(y)}(\lambda), \mathbf{X}^{(z)}(\lambda), \ldots\right] = E\left[\lambda \mathbf{X}_{POL}^{(x)}, \lambda \mathbf{X}_{POL}^{(y)}, \lambda \mathbf{X}_{POL}^{(z)}, \ldots\right]. \tag{8}$$

This parametrization of the energy in terms of  $\mathbf{X}^{(x)}$  is justified since unitary transformations within the fragments' occupied space do not change the total density, thus, once each fragment's density is specified, the total density is determined, so is the energy. Using the fundamental theorem of line integrals, the polarization energy can therefore be decomposed as (see also ref. 46)

$$\Delta E = \int_0^1 \frac{\partial E[\lambda]}{\partial \lambda} \, d\lambda = \int_0^1 \sum_{x,a,i} \frac{\partial E[X]}{\partial X_{ia}^{(x)}} \left( X_{\text{POL}}^{(x)} \right)_{ia} \, d\lambda \tag{9}$$

$$= \sum_{x} \sum_{a,i} \left[ \int_{0}^{1} \frac{\partial E[X]}{\partial X_{ia}^{(x)}} d\lambda \right] \left( X_{\text{POL}}^{(x)} \right)_{ia}$$
 (10)

$$= \sum_{x} \operatorname{Tr} \left\{ \hat{F}_{vo}^{\operatorname{eff}(x)} \left( \hat{X}_{POL}^{(x)} \right)_{ov} \right\}, \tag{11}$$

In the orthonormal MO basis of fragment x, an effective Fock operator is defined as:

$$F_{ai}^{\text{eff}(x)} = \int_0^1 \frac{\partial E[X]}{\partial X_{ia}^{(x)}} \, d\lambda = \int_0^1 F_{ai}^{\text{eff}(x)}(\lambda) \, d\lambda. \tag{12}$$

Using the chain rule, we obtain

$$F_{ai}^{\text{eff}(x)}(\lambda) = \frac{\partial E}{\partial X_{ia}^{(x)}} = \frac{\partial E}{\partial P_{\alpha\beta}} \frac{\partial P_{\alpha\beta}}{\partial X_{ia}^{(x)}} = F_{\alpha\beta} \frac{\partial P_{\alpha\beta}}{\partial X_{ia}^{(x)}},\tag{13}$$

where  $\mathbf{P} = \mathbf{P}(\mathbf{X})$  denotes the total density matrix after we rotate each fragment's MOs by the corresponding  $\mathbf{X}^{(x)}$ , and  $\mathbf{F} = \mathbf{F}(\mathbf{X})$  is the Fock matrix of the rotated system. The matrix elements of  $\mathbf{P}(\mathbf{X})$  are

$$P(X)_{\alpha\beta} = \langle \omega^{\alpha} | \hat{P}(X) | \omega^{\beta} \rangle = \langle \omega^{\alpha} | \psi_{yl}^{(y)}(X) \rangle \sigma_{oo}(X)_{yl,zk}^{-1} \langle \psi_{zk}^{(z)}(X) | \omega^{\beta} \rangle$$
 (14)

$$= C(X)_{\alpha,yl}\sigma_{oo}(X)_{yl,zk}^{-1}C(X)_{\beta,zk}, \tag{15}$$

where C(X) is the MO coefficient matrix after rotation, and  $\sigma_{oo}(X)$  is the overlap matrix of the rotated occupied MOs. Thus,

$$\frac{\partial P(X)_{\alpha\beta}}{\partial X_{ia}^{(x)}} = \frac{\partial C(X)_{\alpha,yl}}{\partial X_{ia}^{(x)}} \sigma_{oo}(X)_{yl,zk}^{-1} C(X)_{\beta,zk}$$
(16)

$$+ C(X)_{\alpha,yl} \frac{\partial \sigma_{oo}(X)_{yl,zk}^{-1}}{\partial X_{ia}^{(x)}} C(X)_{\beta,zk}$$

$$\tag{17}$$

$$+ C(X)_{\alpha,yl}\sigma_{oo}(X)_{yl,zk}^{-1} \frac{\partial C(X)_{\beta,zk}}{\partial X_{io}^{(x)}}$$

$$\tag{18}$$

Using the equality<sup>47</sup>  $\frac{\partial U(X)_{rs}}{\partial X_{ia}} = U(X)_{ri}\delta_{as} - U(X)_{ra}\delta_{is}$ , we have

$$\frac{\partial C(X)_{\alpha,yl}}{\partial X_{ia}^{(x)}} = \frac{\partial}{\partial X_{ia}^{(x)}} \left[ C(0)_{\alpha,yp} U_{yp,yl}^{(y)} \right] = -\delta_{xy} \delta_{li} C(X)_{\alpha,ya}, \tag{19}$$

where C(0) is the MO coefficient matrix of the FRZ state (with no rotation). Similarly,

$$\frac{\partial C(X)_{\beta,zk}}{\partial X_{ia}^{(x)}} = -\delta_{xz}\delta_{ki}C(X)_{\beta,za}.$$
(20)

To evaluate Eqn.(17), we take partial derivative on both sides of  $\sigma_{oo}(X)\sigma_{oo}(X)^{-1} = I$ , which gives

$$\frac{\partial \sigma_{oo}(X)_{yl,zk}^{-1}}{\partial X_{ia}^{(x)}} = -\sigma_{oo}(X)_{yl,wm}^{-1} \frac{\partial \sigma_{oo}(X)_{wm,vn}}{\partial X_{ia}^{(x)}} \sigma_{oo}(X)_{vn,zk}^{-1}$$
(21)

The matrix element of  $\sigma_{oo}(X)$  is

$$\sigma_{oo}(X)_{wm,vn} = \langle \psi_m^{(w)}(X) | \psi_n^{(v)}(X) \rangle = U_{wp,wm}^{(w)} \langle \psi_p^{(w)}(0) | U_{vq,vn}^{(v)} | \psi_q^{(v)}(0) \rangle = U_{wp,wm}^{(w)} \sigma(0)_{wp,vq} U_{vq,vn}^{(v)}$$
(22)

Notice if w=v, the occupied MO overlap matrix is identity and its derivative is 0. To get non-zero derivative, we must have  $w=x, v\neq x$  or  $w\neq x, v=x$ , so

$$\frac{\partial \sigma_{oo}(X)_{wm,vn}}{\partial X_{ia}^{(x)}} = \delta_{wx} (1 - \delta_{vx}) \frac{\partial U_{xp,xm}^{(x)}}{\partial X_{xi,xa}^{(x)}} \sigma(0)_{xp,vq} U_{vq,vn}^{(v)} + (1 - \delta_{wx}) \delta_{vx} U_{wp,wm}^{(w)} \sigma(0)_{wp,xq} \frac{\partial U_{xq,xn}^{(x)}}{\partial X_{xi,xa}^{(x)}}$$
(23)

$$= -\delta_{wx}\delta_{mi}U_{xp,xa}^{(x)}\sigma(0)_{xp,vq}U_{vq,vn}^{(v)} + \delta_{wx}\delta_{vx}\delta_{mi}U_{xp,xa}^{(x)}\sigma(0)_{xp,vq}U_{vq,vn}^{(v)}$$
(24)

$$-\delta_{vx}\delta_{ni}U_{wp,wm}^{(w)}\sigma(0)_{wp,xq}U_{xq,xa}^{(x)} + \delta_{wx}\delta_{vx}\delta_{ni}U_{wp,wm}^{(w)}\sigma(0)_{wp,xq}U_{xq,xa}^{(x)}$$
 (25)

After simplification, we get

$$\frac{\partial P(X)_{\alpha\beta}}{\partial X_{ia}^{(x)}} = -C(X)_{\alpha,xa} \left[ \sigma_{oo}(X)^{-1} C^{(o)}(X)^T \right]_{xi,\beta} - \left[ C^{(o)}(X) \sigma_{oo}(X)^{-1} \right]_{\alpha,xi} C(X)_{\beta,xa}$$
 (26)

+ 
$$\left[C^{(o)}(X)\sigma_{oo}(X)^{-1}\right]_{\alpha,xi} \left[U^{(x)T}\sigma(0)^{(x-)}U(X)^{(-o)}\sigma_{oo}(X)^{-1}C^{(o)}(X)^{T}\right]_{xa,\beta}$$
 (27)

+ 
$$\left[C^{(o)}(X)\sigma_{oo}(X)^{-1}U(X)^{(-o)T}\sigma(0)^{(-x)}U^{(x)}\right]_{\alpha,xa}\left[\sigma_{oo}(X)^{-1}C^{(o)}(X)^{T}\right]_{xi,\beta}$$
, (28)

where  $C^{(o)}(X)$  is the MO coefficient matrix of the rotated occupied MOs,  $\sigma(0)^{(x-)}$  is the FRZ state overlap matrix between MOs of fragment x and all MOs, and  $U(X)^{(-o)}$  is a block diagonal matrix whose blocks are the first occupied number of columns of  $U(X)^{(x)}$  of each fragment, and its structure is shown below

$$U(X)^{(-o)} = \begin{pmatrix} o_1 & o_2 & \cdots & o_{N_f} \\ o_1 + v_1 & U^{(1)} & 0 & 0 & 0 \\ o_2 + v_2 & 0 & 0 & 0 \\ \vdots & \vdots & \vdots & \vdots & \vdots \\ o_{N_f} + v_{N_f} & 0 & 0 & U^{(N_f)} \end{pmatrix}.$$

$$(29)$$

After the contraction with the Fock matrix, we get

$$F_{ai}^{\text{eff}(x)}(\lambda) = F(X)_{\alpha\beta} \frac{\partial P(X)_{\alpha\beta}}{\partial X_{ia}^{(x)}}$$
(30)

$$= 2 \left[ U^{(x)T} \sigma(0)^{(x-)} U(X)^{(-o)} \sigma_{oo}(X)^{-1} C^{(o)}(X)^T F(X) C^{(o)}(X) \sigma_{oo}(X)^{-1} \right]$$
(31)

$$-C(X)^{T}F(X)C^{(o)}(X)\sigma_{oo}(X)^{-1}\Big]_{Ta,Ti}.$$
(32)

Finally, the effective fock matrix is obtained from a numerical integral using a 5-point Gauss-Lobatto quadrature. 40

#### 2.4 Non-perturbative charge decomposition analysis

By definition, the polarization charge transfer is  $\Delta Q = \text{Tr} \Big\{ \hat{P}_{\text{POL}} \hat{Q}_{\text{FRZ}} \Big\}$ . Define  $Q[X(\lambda)] = \text{Tr} \Big\{ \hat{P}(X) \hat{Q}_{\text{FRZ}} \Big\} = Q[X^{(x)}(\lambda), X^{(y)}(\lambda), X^{(z)}(\lambda), \dots] = Q\Big[\lambda X_{\text{POL}}^{(x)}, \lambda X_{\text{POL}}^{(y)}, \lambda X_{\text{POL}}^{(z)}, \dots\Big]$ , and similar to the energy difference, we have

$$\Delta Q = \int_0^1 \frac{\partial Q[\lambda]}{\partial \lambda} \, d\lambda = \int_0^1 \sum_{x,a,i} \frac{\partial Q[X]}{\partial X_{ia}^{(x)}} \left( X_{\text{POL}}^{(x)} \right)_{ia} \, d\lambda \tag{33}$$

$$= \sum_{x} \sum_{a,i} \left[ \int_{0}^{1} \frac{\partial Q[X]}{\partial X_{ia}^{(x)}} d\lambda \right] \left( X_{\text{POL}}^{(x)} \right)_{ia}$$
 (34)

$$= \sum_{x} \operatorname{Tr} \left\{ \hat{P}_{vo}^{\operatorname{eff}(x)} \left( \hat{X}_{POL}^{(x)} \right)_{ov} \right\}, \tag{35}$$

where in the orthonormal basis of fragment x,

$$P_{ai}^{\text{eff}(x)} = \int_0^1 \frac{\partial Q[X]}{\partial X_{ia}^{(x)}} d\lambda = \int_0^1 P_{ai}^{\text{eff}(x)}(\lambda) d\lambda.$$
 (36)

Expand Q[X] in AO basis, we get

$$P_{ai}^{\text{eff}(x)}(\lambda) = \frac{\partial Q[X]}{\partial X_{ia}^{(x)}} = \frac{\partial}{\partial X_{ia}^{(x)}} \left[ P(X) S Q_{\text{FRZ}} S \right]_{\alpha\alpha} = \frac{\partial P(X)_{\alpha\beta}}{\partial X_{ia}^{(x)}} \left( S Q_{\text{FRZ}} S \right)_{\alpha\beta}. \tag{37}$$

This looks exactly the same as the expression for the effective fock matrix, and we just need to replace F(X) with  $SQ_{FRZ}S$  to get

$$P_{ai}^{\text{eff}(x)}(\lambda) = 2 \left[ U^{(x)T} \sigma(0)^{(x-)} U(X)^{(-o)} \sigma_{oo}(X)^{-1} C^{(o)}(X)^T S Q_{\text{FRZ}} S C^{(o)}(X) \sigma_{oo}(X)^{-1} \right]$$
(38)

$$-C(X)^T SQ_{FRZ} SC^{(o)}(X) \sigma_{oo}(X)^{-1} \Big]_{ra, ri}. \tag{39}$$

Finally, the effective density matrix is obtained using the same numerical integration procedure.

# 2.5 Fragment-wise complementary occupied-virtual pairs (COVPs) analysis

From Eqs. 7, one can see that the polarization energy and charge flow of each fragment have contributions from  $o_x$  occupied orbitals coupling to  $v_x$  virtual orbitals, and generally no occupied-virtual pairs can be omitted. However, it is obvious that the rotations of occupied space and virtual space of each fragment will not change the fragment polarization energy or electron flow. This invariance can be utilized to optimally compress the orbital representation of the polarization process by singular value decomposition. Define a set of rotated occupied and virtual orbitals

$$|\psi'_{xi}\rangle = \sum_{xj}^{o_x} U_{xj,xi}^{(x)} |\psi_{xj}\rangle \tag{40}$$

$$|\psi'_{xa}\rangle = \sum_{xb}^{v_x} V_{xb,xa}^{(x)} |\psi_{xb}\rangle. \tag{41}$$

Since this does not change the fragment polarization energy and charge transfer, we have

$$\Delta E^{(x)} = \sum_{ia} \langle \psi'_{xa} | \hat{F}_{vo}^{\text{eff}} | \psi'_{xi} \rangle \langle \psi'_{xi} | \left( \hat{X}_{POL}^{(x)} \right)_{ov} | \psi'_{xa} \rangle$$
(42)

$$\Delta Q^{(x)} = \sum_{ia} \langle \psi'_{xa} | \hat{P}_{vo}^{\text{eff}} | \psi'_{xi} \rangle \langle \psi'_{xi} | \left( \hat{X}_{\text{POL}}^{(x)} \right)_{ov} | \psi'_{xa} \rangle. \tag{43}$$

Notice that under the new basis, the matrix element of  $\hat{X}_{\text{POL}}^{(x)}$  is

$$\langle \psi'_{xi} | \left( \hat{X}_{POL}^{(x)} \right)_{ov} | \psi'_{xa} \rangle = \sum_{ib} U_{xi,xj}^{(x)T} \langle \psi_{xj} | \left( \hat{X}_{POL}^{(x)} \right)_{ov} | \psi_{xb} \rangle V_{xb,xa}^{(x)} = \left[ U^{(x)T} X_{ov}^{(x)} V^{(x)} \right]_{xi,xa}$$
(44)

If we rotate the occupied space and virtual space using the left and right orthonormal matrices in the singular value decomposition (SVD) of  $\langle \psi_{xj} | \left( \hat{X}_{\text{POL}}^{(x)} \right)_{ov} | \psi_{xb} \rangle$ ,  $\left( \hat{X}_{\text{POL}}^{(x)} \right)_{ov}$  will be represented by a rectangular diagonal matrix with at most min $\{o_x, v_x\}$  non-zero entries.

The min $\{o_x, v_x\}$  pairs of the corresponding occupied and projected virtual orbitals obtained in this way are called the complementary occupied-virtual pairs (COVPs), and they give the most compact description of the polarization energy and charge transfer of fragment x during the polarization process. It is worth noticing that both the occupied and virtual COVPs thus constructed for the POL analysis are still localized on each fragment, and are non-orthogonal to the polarization COVPs on other fragments (just as the ALMOs are). This is in contrast with the COVPs of the CT analysis,  $^{39,40}$  which can delocalize to other fragments due to their orthogonalization tails.

The interpretation of the COVPs is that electrons move from the occupied orbital to the virtual orbital, and electron density decreases in regions where the COVPs are out of phase, while the electron density increases in regions where the COVPs are in phase. To achieve the above convention of interpretation, in practice, we multiply all the operators of Eq. (42) and (43) by -1 and construct the COVPs by doing the SVD of  $-\left(\hat{X}_{\text{POL}}^{(x)}\right)_{ov}$ . It is obvious the expressions of the energy transfer and charge transfer associated with each COVP are unchanged, but this practice allows us to interpret the COVPs as described before, and the reasoning is shown in the next subsection.

# 2.6 Analysis of the COVP phase and electron flow on a toy model

To understand the relationship between the COVP phase and the direction of electron flow during polarization (the same reasoning can be applied to the CT process<sup>40</sup> as well), we

analyze a simple toy model of the polarization of a hydrogen atom in a uniform electric field, as shown in Fig. 1. Let us assume the electric field is weak and oriented along the z axis,  $\vec{E} = E\hat{z}$  and that the H atom is located at the origin of the coordinate system. Therefore, the total Hamiltonian is

$$\hat{H} = \hat{H}_0 - \hat{\vec{\mu}} \cdot \vec{E},\tag{45}$$

where  $\hat{H}_0$  is the non-relativistic H atom Hamiltonian. The field-induced perturbation is

$$\hat{H}_1 = -\hat{\vec{\mu}} \cdot \vec{E} = -\left(-e\hat{\vec{r}}\right) \cdot E\hat{z} = eEz,\tag{46}$$

where e is the magnitude of electron charge, and  $\vec{r}$  is its position.

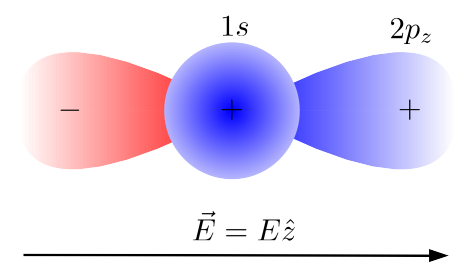


Figure 1: H atom in uniform electric field.

It is sufficient to allow a single virtual orbital to describe polarization, and by symmetry, referring to Fig. 1, a  $|2p_z\rangle$  orbital is suitable to polarize a  $|1s\rangle$  ground state H atom. Our model Hilbert space will therefore be 2-dimensional:  $\{|1s\rangle, |2p_z\rangle\}$  The frozen wavefunction corresponding to the isolated H atom fragment is simply:

$$|\psi_{\text{FRZ}}\rangle = |\psi_0^{(0)}\rangle = |1s\rangle,$$
 (47)

We assume the phases of  $|1s\rangle$  and  $|2p_z\rangle$  are as indicated in Fig. 1.

The first order correction to the wavefunction under the perturbation is

$$|\psi_0^{(1)}\rangle = \sum_{k \neq 1s} \frac{\langle \psi_k | \hat{H}_1 | 1s \rangle}{E_{1s} - E_k} |\psi_k\rangle = eE \frac{\langle 2p_z | z | 1s \rangle}{E_{1s} - E_{2p_z}} |2p_z\rangle. \tag{48}$$

With positive numerator and negative denominator, the coefficient of  $|2p_z\rangle$  is negative. Therefore our normalized perturbed wavefunction (which is the POL state) is of the form

$$|\psi_{\text{POL}}\rangle = \cos\theta |1s\rangle - \sin\theta |2p_z\rangle,$$
 (49)

where  $\theta \in (0, \pi/2)$ . This suggests the polarized state shifts in the  $-\hat{z}$  direction, which is expected since the electron is attracted towards the positive field direction.

The density operators of these two states,  $\hat{P}_{FRZ} = |\psi_{FRZ}\rangle\langle\psi_{FRZ}|$  and  $\hat{P}_{POL} = |\psi_{POL}\rangle\langle\psi_{POL}|$  have the following matrix representations:

$$\mathbf{P}_{\text{FRZ}} = \begin{array}{c} |1s\rangle & |2p_z\rangle \\ \mathbf{P}_{\text{FRZ}} = & |1s\rangle \begin{pmatrix} 1 & 0 \\ 0 & 0 \end{pmatrix}$$
 (50)

$$\mathbf{P}_{POL} = \begin{vmatrix} |1s\rangle & |2p_z\rangle \\ |2p_z\rangle & -\sin\theta\cos\theta \\ |2p_z\rangle & -\sin\theta\cos\theta \end{vmatrix}$$

$$(51)$$

By the relationship  $\mathbf{P}_{POL} = \mathbf{U}(\mathbf{X})\mathbf{P}_{FRZ}\mathbf{U}(\mathbf{X})^T$ , it's easy to see that

$$\mathbf{U}(\mathbf{X}) = \begin{pmatrix} \cos \theta & \sin \theta \\ -\sin \theta & \cos \theta \end{pmatrix} \tag{52}$$

From the definition,  $U(X) = \exp(X)$ , so we have

$$\mathbf{X} = \begin{pmatrix} 0 & \theta \\ -\theta & 0 \end{pmatrix} \tag{53}$$

Thus the ov block of **X** is simply  $X_{ov} = \theta$ . Its trivial SVD gives the occupied COVP as

 $|1s\rangle$  and the virtual COVP as  $|2p_z\rangle$  (no compression is possible). However the phases are significant. Comparing the COVPs (or the original orbitals), we can see electrons move from the region where COVPs are in phase to the region where COVPs are out of phase.

Since this is not an intuitive convention, we instead construct the COVPs using  $-\mathbf{X}_{ov}$ . As the singular values are by definition always positive, the overall minus sign will be incorporated in either the occupied or the virtual COVPs, which will change their relative phases. With this phase convention for the COVPs, electrons move from the region where COVPs are out of phase to the region where COVPs are in phase. This convention will facilitate chemical interpretation.

# 3 Computational details

Isolated fragment SCF calculations were first performed, after which the block diagonal MO coefficient matrix and the density matrix  $P_{\text{FRZ}}$  of the frozen state were constructed using the occupied orbitals and DQ-FERFs of each fragment. We then ran SCF-MI calculations to obtain the polarized state and the density matrix  $P_{\text{POL}}$ . The generator  $\mathbf{X}$  of the unitary transformation connecting FRZ and POL states was obtained by minimizing the cost function  $C = \|P_{\text{POL}} - U(X)P_{\text{FRZ}}U(X)^T\|_F^2$  as in reference 40. For UHF calculations, the above procedures were performed for the  $\alpha$  and  $\beta$  spin separately, since the density matrices do not couple orbitals with different spins.

The polarization analysis algorithm was implemented in a development version of the Q-Chem quantum chemistry program. <sup>48</sup> The  $\omega$ B97X-D functional <sup>49</sup> with the def2-TZVPD basis set <sup>50,51</sup> were used for geometry optimization and vibrational mode analysis.  $\omega$ B97X-D/aug-cc-pVTZ<sup>52-54</sup> single point calculations were used for the energy decomposition analysis unless otherwise specified. Geometries of all molecules were confirmed to be local minima on the potential energy surface by confirming that the Hessian matrix has no negative eigenvalues. All the COVPs were plotted with isosurface value of  $\pm 0.07$  a.u., and all the molecular figures

were plotted using IQmol. The occupied and virtual COVPs were plotted in transparent solid and wire-frame style respectively. All plots were generated using Matplotlib.<sup>55</sup>

#### 4 Results and discussion

#### $4.1 \quad \text{He} - \text{Li}^+$

We first consider the interaction between a He atom and a Li<sup>+</sup> cation, which has an equilibrium distance of 1.92 Å. At large distances, this inter-molecular interaction is expected to be polarization dominated due to the large difference between the first ionization energies (IE) of He (24.6 eV)<sup>56</sup> and Li (5.4 eV),<sup>57</sup> which makes the electron transfer from He to Li<sup>+</sup> unfavorable. We performed a series of EDA calculations with the inter-atomic distance  $r_{\text{He-Li}^+}$  increasing from 1.8 Å to 6.0 Åwith increment of 0.3 Å. From Figure 2(a) and 2(b), it is obvious that the total energy decreases of the POL and CT processes obtained from ALMO EDA agree very well with those obtained by direct subtraction, which confirms that the 5-point quadrature used to construct the effective Fock matrices is satisfactory. Both POL and CT energies approach 0 as  $r_{\text{He-Li}^+}$  increases, and the magnitude of  $\Delta E_{\text{POL}}$  remains dominant over  $\Delta E_{\text{CT}}$  (Figure 2(c)), indicating the polarization dominant nature of this inter-molecular interaction. The polarization energy is all due to the polarization of He, as one would expect, and Figure 2(d) shows the slope of the log-log plot of the polarization energy with respect to distance plot is very close to -4, which is the correct asymptotic behavior of a charge-induced dipole interaction.

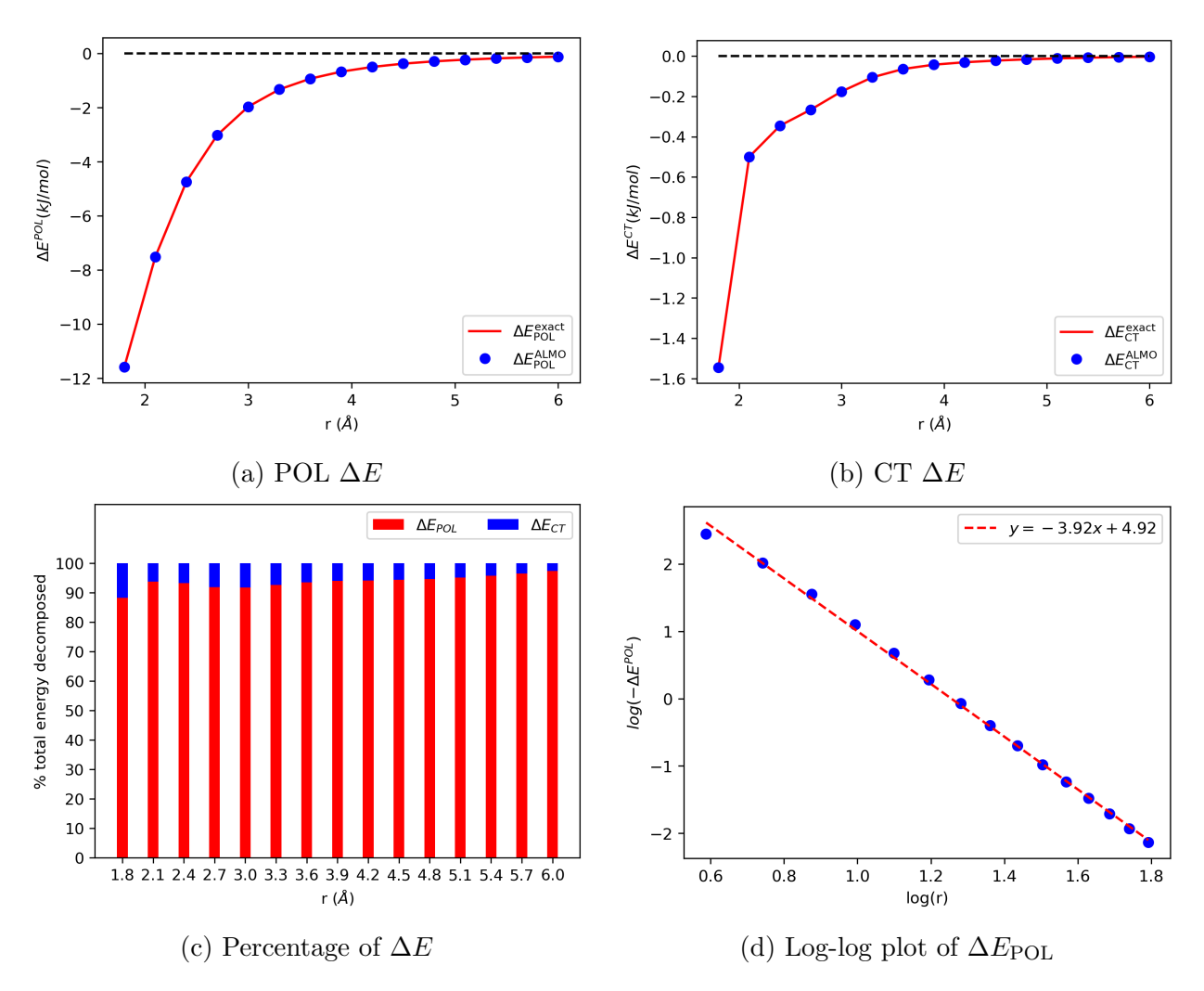


Figure 2: (a) Energy decrease in the POL process obtained from  $E_{\rm POL}-E_{\rm FRZ}$  ( $\Delta E_{\rm POL}^{\rm exact}$  in red line) and ALMO EDA ( $\Delta E_{\rm POL}^{\rm ALMO}$  in blue dots) as a function of  $r_{\rm He-Li^+}$ . (b) Energy decrease in the CT process obtained from  $E_{\rm CT}-E_{\rm POL}$  ( $\Delta E_{\rm CT}^{\rm exact}$  in red line) and ALMO EDA ( $\Delta E_{\rm CT}^{\rm ALMO}$  in blue dots) as a function of  $r_{\rm He-Li^+}$ . (c) Percentage of  $\Delta E_{\rm POL}$  and  $\Delta E_{\rm CT}$  out of  $\Delta E_{\rm POL}+\Delta E_{\rm CT}$  in the relaxation from FRZ to CT as a function of  $r_{\rm He-Li^+}$ . (d) log-log plot of the magnitude of the polarization energy with respect to distance.

The POL energy at all distances can be described by a single COVP with 100% energy contribution, such as the one at  $r_{\rm He-Li^+}=3.9$  Å system shown in Figure 3. It is clear that this COVP describes the local charge flow from the He 1s orbital to its virtual  $2p_z$  orbital that is oriented towards the Li<sup>+</sup>. Moreover, the relative phases of the 1s orbital and the  $2p_z$  orbital indicates the electrons flow from left to right due to the electrostatic attraction exerted by the positively charged Li<sup>+</sup>. The compact description of the polarization of He

by only one COVP is due to the fact that there is only one occupied molecular orbital (for restricted SCF calculation) in He.



Figure 3: The COVP of the POL process of the He – Li<sup>+</sup> system at  $r_{\rm He-Li^+}=3.9$  Å.

#### $4.2 ext{Ne} - Ar^+$

We consider the interaction between a Ne atom and an Ar<sup>+</sup> cation, which has an equilibrium distance of 2.9 Å at the level of HF/aug-cc-pVTZ. The reason for choosing HF as the electronic structure method is that this problem is expected to be self-interaction sensitive due to the presence of an odd hole (on Ar). Due to the larger IE of Ne (21.6 eV)<sup>57</sup> than Ar (15.8 eV),<sup>58</sup> we expect this inter-molecular interaction to be CT dominated at short distances, and POL dominated at large distances. From Figure 4(a) and 4(b), it is obvious that the total energy contributions of the POL and CT processes obtained from ALMO EDA agree very well with those obtained by direct subtraction, which again confirms the effectiveness of our POL and CT decomposition methods. Figure 4(c) shows that CT contributes more than POL at short distances, while at larger distances POL dominates the binding process, as expected.

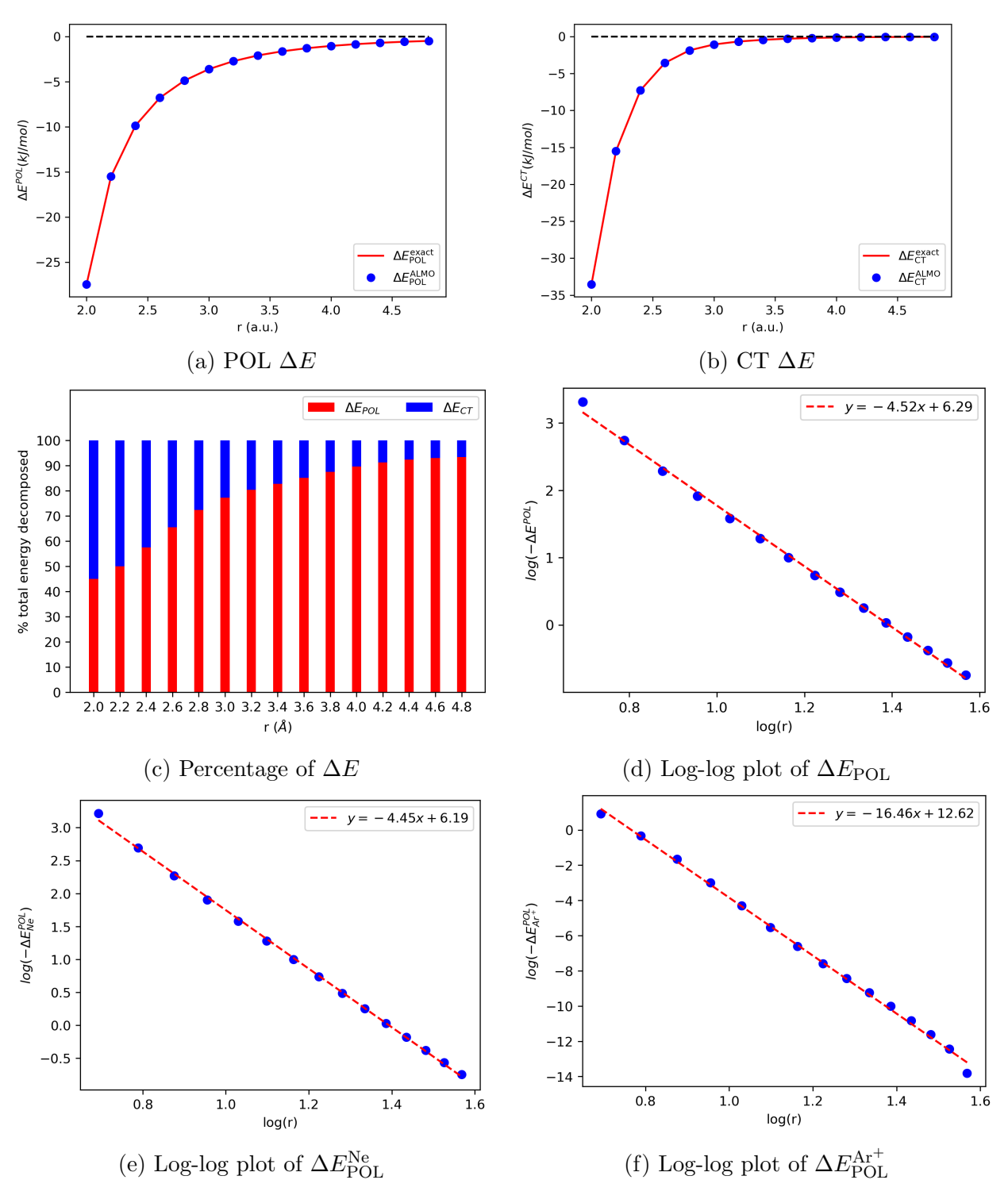


Figure 4: (a) POL energy decrease,  $E_{\rm POL} - E_{\rm FRZ}$  ( $\Delta E_{\rm POL}^{\rm exact}$ : red line) and ALMO EDA ( $\Delta E_{\rm POL}^{\rm ALMO}$ : blue dots) as a function of  $r_{\rm Ne-Ar^+}$ . (b) CT energy decrease obtained from  $E_{\rm CT} - E_{\rm POL}$  ( $\Delta E_{\rm CT}^{\rm exact}$ : red line) and ALMO EDA ( $\Delta E_{\rm CT}^{\rm ALMO}$ : blue dots) as a function of  $r_{\rm Ne-Ar^+}$ . (c) Percentage of  $\Delta E_{\rm POL}$  and  $\Delta E_{\rm CT}$  out of  $\Delta E_{\rm POL} + \Delta E_{\rm CT}$  in the relaxation from FRZ to CT as a function of  $r_{\rm Ne-Ar^+}$ . (d) log-log plot of  $E_{\rm POL}$  vs r (e) log-log plot of  $E_{\rm POL}$  of Ne vs r (f) log-log plot of  $E_{\rm POL}$  of Ar<sup>+</sup> vs r; the red dashed line is the best linear fit in panels (d)-(f).

The different distance dependence (polynomial versus approximately exponential) of POL and CT is visually evident (examined in more detail for the  $H_2O \cdots Cl^-$  interaction below). Figure 4 (d) shows the polarization energy roughly agrees with the  $r^{-4}$  distance dependence of charge - induced dipole interaction, as is the polarization energy of Ne in Figure 4 (e). The fact that the slope is larger in magnitude than -4 indicates additional short-range contributions that decay more rapidly – for instance due to overlap effects. Likewise, Figure 4(f) shows the very rapid decay of weak polarization effects on  $Ar^+$  due to interaction with the (polarized) Ne atom.

To illustrate the details of the binding process of this cluster, we show the EDA and COVP analysis results at the distance of 2.8 Å. EDA results of Table 1a shows that POL energy is the dominant contribution to binding energy, and table 1b shows two significant COVPs that contribute 60% of the POL energy. Figure 5 indicates the polarization is achieved by electrons moving from the  $2p_z$  orbital of Ne into its empty  $3d_{z^2}$  orbital, and the phase convention shows the result of polarization of Ne is an increased electron density at the end closer to  $Ar^+$  and a decreased electron density at the opposite end due to the electron static attraction of the positively charged  $Ar^+$ . Relatively weak polarization despite the strong perturbation of an unscreened charge reflects the high cost of changing the principal quantum number in the POL process. Table 1c shows two significant COVPs in the CT process that contributes 80% of the CT energy, and figure 5 shows the dominant COVP demonstrates donation of electrons from the  $2p_z$  orbital of Ne into the empty  $3p_z$  orbital of  $Ar^+$ , while the smaller COVP shows donation of electrons from the  $2p_z$  orbital of Ne into the empty  $3d_{z^2}$  orbital of  $Ar^+$ , which is lower in energy.

Table 1: (a) Energies (in kJ/mol) and amounts of transferred charge (in me<sup>-</sup>) calculated using ALMO EDA.  $\Delta E_{\rm ele+Pauli}$  corresponds to the sum of energy decreases due to electrostatic interaction and Pauli repulsion,  $\Delta E_{\rm disp}$  corresponds to the dispersion energy, and  $\Delta E_{\rm int}$  is the total interaction energy.  $\Delta E_{\rm POL}$  and  $\Delta E_{\rm CT}$  are calculated using the non-perturbative EDA method. (b, c) Significant COVPs of the POL and CT process, as well as their associated energy decrease (in kJ/mol), amounts of transferred charge (in me<sup>-</sup>) and their contributions in percentage.

$\Delta E_{\text{ele+Pauli}}$	$\Delta E_{\rm disp}$	$\Delta E_{ m POL}$	$\Delta Q_{ m POL}$	$\Delta E_{\mathrm{CT}}$	$\Delta Q_{\mathrm{CT}}$	$\Delta E_{\mathrm{int}}$
3.02	-1.53	-4.88	1.37	-1.86	1.30	-5.25
		/ \ DI	) A 1,			

(a) EDA results

Pair	Donor	Acceptor	$\Delta E$	$\Delta E/\Delta E_{ m POL}(\%)$	$\Delta Q$	$\Delta Q/\Delta Q_{ m POL}(\%)$
$\alpha 1$	Ne	Ne	-1.33	27.22	0.41	29.54
$\beta 1$	Ne	Ne	-1.64	33.56	0.57	41.25

(b) Significant COVPs of POL process

Pair	Donor	Acceptor	$\Delta E$	$\Delta E/\Delta E_{\rm CT}(\%)$	$\Delta Q$	$\Delta Q/\Delta Q_{\mathrm{CT}}(\%)$
$\alpha 2$	Ne	$Ar^+$	-0.26	14.22	0.08	6.51
$\beta 2$	Ne	$\mathrm{Ar}^{+}$	-1.21	65.32	1.18	90.44

(c) Significant COVPs of CT process

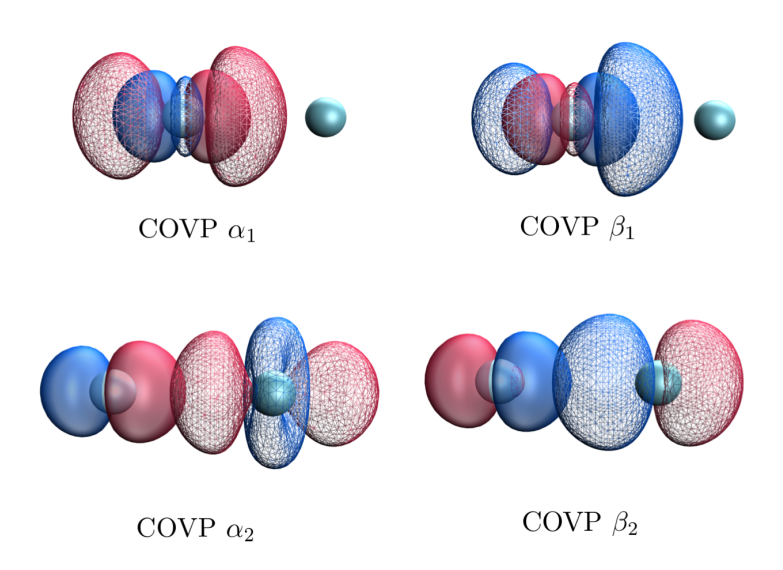


Figure 5: Plots of significant COVPs of Ne-Ar<sup>+</sup> in the POL and CT process.

## 4.3 $H_2O - Cl^-$

We next consider the interaction between a  $H_2O$  molecule and a  $Cl^-$  anion. The structure was optimized at the RIMP2/cc-pVDZ level and frequency analysis was performed at the same level of theory to confirm that a minimum was found. EDA calculations at HF/aug-cc-pVTZ was then performed on different structures obtained by increasing the distance between the O atom and  $Cl^-$ , where the minimal distance at about 3.1 Å corresponds to the equilibrium geometry. Figure 6 (a) shows agreement between the POL energy obtained from our EDA method and direct energy subtraction. Subplot (b) shows a roughly  $1/r^4$  distance dependence of the POL energy, which is the correct asymptotic behavior of the charge-induced dipole interaction (i.e. polarization of water by  $Cl^-$ ).

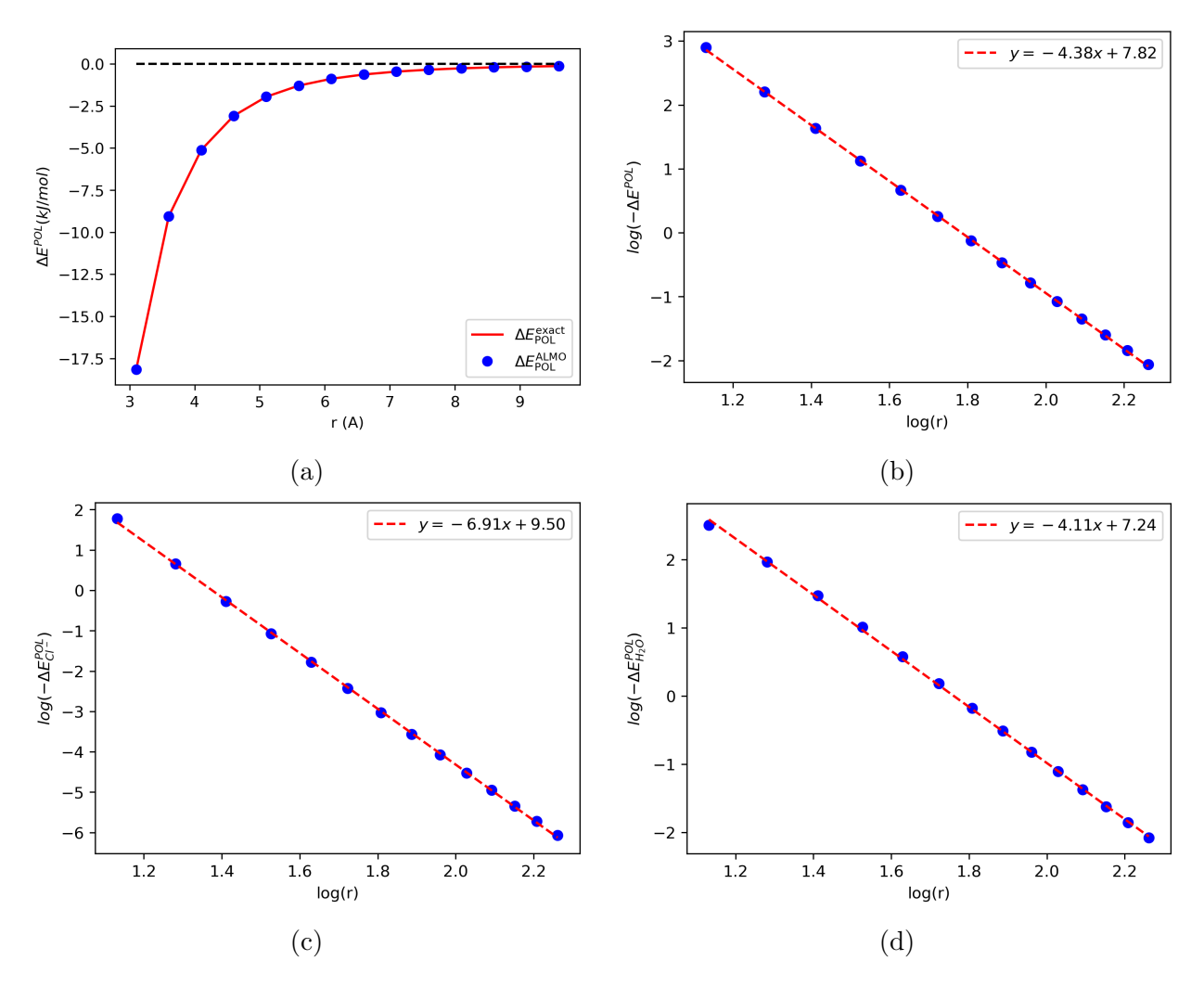


Figure 6: (a) Energy decrease in the POL process obtained from  $E_{\rm POL} - E_{\rm FRZ}$  ( $\Delta E_{\rm POL}^{\rm exact}$  in red line) and ALMO EDA ( $\Delta E_{\rm POL}^{\rm ALMO}$  in blue dots) as a function of r, the distance between O and Cl. (b) log-log plot of the polarization energy and r, the red dashed line is the best linear fit. (c) log-log plot of the polarization energy of Cl<sup>-</sup> and r, the red dashed line is the best linear fit. (d) log-log plot of the polarization energy of H<sub>2</sub>O and r, the red dashed line is the best linear fit.

By contrast, subplot (c) shows that the distance dependence of the POL energy contribution from Cl<sup>-</sup> is about  $1/r^{6.9}$ . This is expected since the polarization of Cl<sup>-</sup> is due to the external dipole moment generated by the H<sub>2</sub>O molecule, and the leading dipole-induced dipole interaction has an asymptotic behavior of  $1/r^6$ . Subplot (d) indicates that the polarization energy of the H<sub>2</sub>O molecule is asymptotically  $1/r^4$ , which is correct for the charge-induced dipole interaction and is the main contribution to the POL energy of this sys-

tem. Therefore, this example demonstrates that our polarization analysis gives the correct asymptotic distance dependence of not only the total POL energy, but also the contributions from each fragment.

#### 4.4 $H_2O$ dimer

It is well known that the hydrogen-bonding in the water dimer weakens the OH bond of the proton donor and thus causes an elongation of its bond length and a red shift in the stretch frequency.  $^{59-62}$  We use a water dimer in vacuum as an example to understand the weakened OH bond using the POL and CT analysis of ALMO EDA. Our calculations show that a free water molecule has an OH bond length of 0.958 Å. In the water dimer, the proton donor OH bond lengths by  $\sim 1\%$  to 0.967 Å, while the other three OH bonds remain almost unchanged. The main EDA results are summarized in Table 2, showing that POL is almost as important as CT in terms of energetic contributions, and a similar number of electrons are rearranged.

Table 2: Energies (in kJ/mol) and amounts of transferred charge (in me<sup>-</sup>) calculated using ALMO EDA.  $\Delta E_{\rm ele+Pauli}$  corresponds to the sum of energy decreases due to electrostatic interaction and Pauli repulsion,  $\Delta E_{\rm disp}$  corresponds to the dispersion energy, and  $\Delta E_{\rm int}$  is the total interaction energy.  $\Delta E_{\rm POL}$  and  $\Delta E_{\rm CT}$  are calculated using the non-perturbative EDA method.

$\Delta E_{\text{ele+Pauli}}$	$\Delta E_{\rm disp}$	$\Delta E_{ m POL}$	$\Delta Q_{ m POL}$	$\Delta E_{\mathrm{CT}}$	$\Delta Q_{\mathrm{CT}}$	$\Delta E_{\mathrm{int}}$
-2.59	-5.49	-5.36	2.73	-7.77	2.95	-21.20

Fragment-wise EDA was then performed to reveal the directions of the energy and charge transfer. To distinguish the two water molecules, we denote the proton donor as "HD" and the proton acceptor as "HA". Table 3a summarizes the POL analysis and Table 3b summarizes the CT analysis. The fragment-wise energy and charge decomposition indicates that the polarization of the proton acceptor accounts for 75% of the energy decrease during the POL process. In the CT process, nearly all the energy decrease is due to the electron flow from the proton acceptor to the proton donor, in the opposite direction of the proton

transfer.

Table 3: Fragment-wise energy decrease (in kJ/mol) and the amount of transferred charge (in  $me^-$ ), and their contributions in percentage in the POL and CT process.

Fragment	$\Delta E$	$\Delta E/\Delta E_{ m POL}(\%)$	$\Delta Q$	$\Delta Q/\Delta Q_{ m POL}(\%)$
HD	-1.47	27.43	0.96	35.16
HA	-3.89	72.57	1.77	64.84

(a) Fragment-wise energy and charge decomposition for the POL process.

Donor	Acceptor	$\Delta E$	$\Delta E/\Delta E_{\rm CT}(\%)$	$\Delta Q$	$\Delta Q/\Delta Q_{\mathrm{CT}}(\%)$
HD	HD	-0.08	1.03	0.01	0.34
HD	HA	-0.50	6.44	0.19	6.44
HA	$_{ m HD}$	-7.17	92.28	3.48	117.97
HA	HA	-0.02	0.26	-0.73	-24.75

<sup>(</sup>b) Fragment-wise energy and charge decomposition for the CT process.

To obtain additional insight, we must perform COVP analysis as summarized in Tables 4a and 4b. Figure 7 illustrates the details of the electron rearrangement. There are two significant COVPs for the POL process, one pair for each of the two water molecules. For the more polarizable water (HA), COVP 1 describes the polarization of the oxygen lone pair electrons towards the donor proton, as a result of electrostatic attraction towards the partially positively charged hydrogen. We can thus clearly identify COVP 1 as achieving energy lowering by electrical polarization.

COVP 2 is only 1/3 the strength, but its character is at least equally interesting. It describes the polarization of the OH  $\sigma$  bond of the proton donor, which is a hybridization of the oxygen 2p orbital and hydrogen 1s orbital. The relative phases of the occupied and virtual orbitals indicates that electrons move away from the proton acceptor along the OH bond. There are two synergistic reasons that we can identify for this behavior. First, is increasing the polarity of the O-H<sub>D</sub> bond to increase the electrostatic induction. Second, is relief of the Pauli repulsion exerted by the adjacent oxygen lone pair of the proton acceptor.

Table 4: Significant COVPs of the POL and CT process, as well as their associated energy decrease (in kJ/mol), amounts of transferred charge (in  $me^-$ ) and their contributions in percentage.

Pair	Donor	Acceptor	$\Delta E$	$\Delta E/\Delta E_{ m POL}(\%)$	$\Delta Q$	$\Delta Q/\Delta Q_{ m POL}(\%)$
1	HA	HA	-3.24	60.50	1.47	53.97
2	HD	HD	-1.07	19.89	0.71	26.18

(a) Significant COVPs of POL process

Pair	Donor	Acceptor	$\Delta E$	$\Delta E/\Delta E_{\rm CT}(\%)$	$\Delta Q$	$\Delta Q/\Delta Q_{\mathrm{CT}}(\%)$
3	НА	HD	-6.90	88.84	3.41	115.73

(b) Significant COVPs of CT process

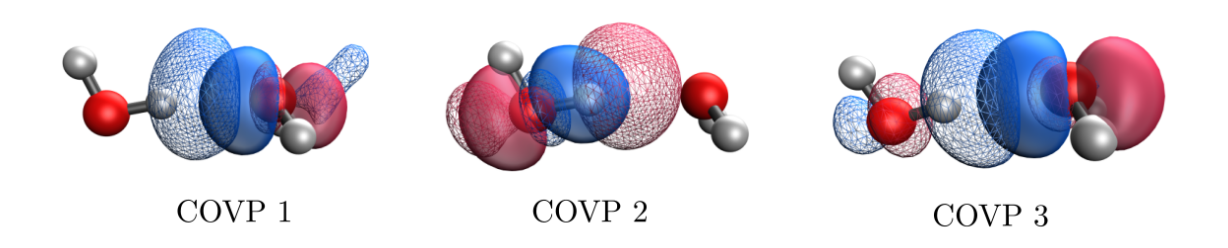


Figure 7: Plots of significant COVPs of water dimer in the POL and CT process.

The charge transfer process is compactly described by one COVP, which shows electron transfer from the proton acceptor to the proton donor (Table 4b). Consistent with previous analysis,  $^{39}$  COVP 3 of Figure (7) clearly shows electron transfer from the oxygen lone pair of the proton acceptor to the O $-H_D$   $\sigma^*$  anti-bonding orbital of the proton donor. This is the main origin of the weakened OH bond, as indicated by its much larger energy decrease (than associated with POL on the proton donor water, which is the only other candidate). The dominance of CT in O $-H_D$  bond weakening has also been clearly identified using the adiabatic EDA.  $^{12,62}$ 

# 4.5 Complex of the 9-fluorenyl radical with Na<sup>+</sup>

Polycyclic aromatic hydrocarbons (PAHs) in their neutral, ionized, hydrogenated and dehydrogenated forms have been proposed as potential sources for the unidentified infrared (UIR) emission bands of some carbon-rich interstellar sources as well as the diffuse interstellar visible absorption bands (DIBs).  $^{63-67}$  With a delocalized  $\pi$  electron framework, they are also far more polarizable than non-conjugated organic molecules, and therefore are also of interest for their non-linear optical properties and singlet fission.  $^{68,69}$  From the standpoint of intermolecular interactions, this means that the POL process can be quite important in stabilizing complexes. With this in mind, we studied the interaction of a 9-fluorenyl radical (FR) with a sodium cation on top of its five-membered ring. Since the isolated PAH has no significant electrical moments, this will serve as an example of polarization-dominant inter-molecular interaction.

ALMO-EDA results (Table 5) indicate that the POL process is indeed the dominant factor in relaxing the two fragments, while the CT energy is of negligible importance. This is expected based on the innocent character of the Na<sup>+</sup> cation, in contrast to the Li<sup>+</sup> ion, <sup>70</sup> and we shall not consider CT further here. Relative to the water dimer, we see that the polarization energy lowering is ~ 15 times larger than the water dimer, and more than 4 times larger than in the chloride-water complex. The COVP analysis of the polarization process (Table 7) clearly demonstrates that the polarization of FR cannot be compactly described by only a few of the COVPs, and the energy decrease as well as the amount of transferred charge are distributed among the six COVPs listed in Table.6, which only accounts for about sixty percent of the total energy and transferred charge of the POL process.

Table 5: Energies (in kJ/mol) and amounts of transferred charge (in me<sup>-</sup>) calculated using ALMO EDA.  $\Delta E_{\rm ele+Pauli}$  corresponds to the sum of energy decreases due to electrostatic interaction and Pauli repulsion,  $\Delta E_{\rm disp}$  corresponds to the dispersion energy, and  $\Delta E_{\rm int}$  is the total interaction energy.  $\Delta E_{\rm POL}$  and  $\Delta E_{\rm CT}$  are calculated using the non-perturbative EDA method.

	$\Delta E_{\text{ele+Pauli}}$	$\Delta E_{\rm disp}$	$\Delta E_{ m POL}$	$\Delta Q_{ m POL}$	$\Delta E_{\rm CT}$	$\Delta Q_{\mathrm{CT}}$	$\Delta E_{ m int}$
Ī	-25.12	-14.15	-79.98	44.20	-2.09	0.54	-121.34

The fragment-wise energy and charge decomposition (Table 6) shows that the polarization process is solely due to the polarization of FR. This is unsurprising given that Na<sup>+</sup> is not polarizable. More surprisingly, FR exhibits nearly equal contributions from the  $\alpha$  and  $\beta$  spins. This is quite interesting as one might have expected significantly larger polarization in one spin sector over the other due to the presence of an odd electron (or hole). Conversely the lack of such a difference is consistent with FR being a relatively stable organic radical.

Table 6: Fragment-wise energy decrease (in kJ/mol) and the amounts of transferred charge (in me<sup>-</sup>), and their precentage contributions in the POL process. The subscripts  $\alpha$  and  $\beta$  denote the  $\alpha$  and  $\beta$  electronic space, respectively.

Fragment	$\Delta E_{\alpha}$	$\frac{\Delta E_{\alpha}}{\Delta E_{\rm POL}}$	$\Delta E_{\beta}$	$\frac{\Delta E_{\beta}}{\Delta E_{\text{POL}}}$	$\Delta Q_{\alpha}$	$\frac{\Delta Q_{\alpha}}{\Delta Q_{\rm POL}}$	$\Delta Q_{\beta}$	$\frac{\Delta Q_{eta}}{\Delta Q_{ m POL}}$
FR	-39.49	49.37	-40.43	50.55	20.72	46.88	23.45	53.05
Na <sup>+</sup>	-0.03	0.04	-0.04	0.05	0.01	0.02	0.01	0.02

Turning to the COVP analysis summarized in Table 7, it is evident that the polarization of FR cannot be compactly described by only a few COVPs. The energy decrease as well as the amount of transferred charge are distributed among the six COVPs listed in Table 7, which only accounts for about 60% of the total energy and transferred charge of the POL process. POL is clearly a collective property of the  $\pi$  system, rather than belonging to one or two more polarizable orbitals.

Table 7: Significant COVPs of the POL process, as well as their associated energy decrease (in kJ/mol), amounts of transferred charge (in me<sup>-</sup>) and their contributions in percentage.  $\alpha$  and  $\beta$  denote the COVPs of  $\alpha$  and  $\beta$  electronic space, respectively.

Pair	Donor	Acceptor	$\Delta E$	$\Delta E/\Delta E_{ m POL}(\%)$	$\Delta Q$	$\Delta Q/\Delta Q_{ m POL}(\%)$
$\alpha_1$	FR	FR	-9.46	11.82	5.62	12.71
$\alpha_2$	FR	FR	-7.77	9.71	4.72	10.68
$\alpha_3$	FR	FR	-5.81	7.26	3.51	7.95
$\beta_1$	FR	FR	-9.20	11.51	7.73	17.49
$\beta_2$	FR	FR	-8.61	10.76	5.11	11.57
$\beta_3$	FR	FR	-7.60	9.50	4.53	10.24

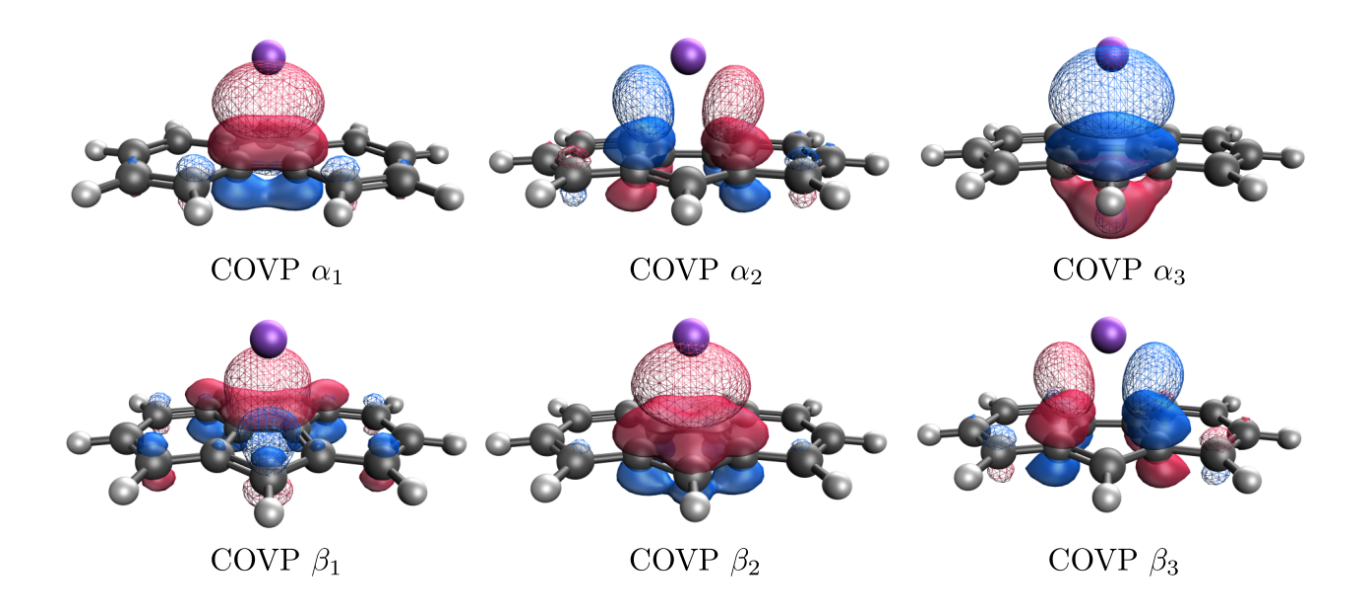


Figure 8: Isosurface plots of the 6 most significant COVPs of 9-fluorenyl radical and Na<sup>+</sup> in the POL process.

Figure 8 shows the significant COVPs of the POL process. The COVPs are mostly localized around the five-membered ring, above which the Na<sup>+</sup> is located. This behavior is expected since the five-membered ring is closer to Na<sup>+</sup> compared to other atoms of FR, so that the electrons in this region feel a stronger electric field exerted by Na<sup>+</sup> and are easier to polarize. Another interesting observation is that all the COVP virtuals are located above their paired occupied orbitals, closer to the Na<sup>+</sup>. Together with the paired phases, this clearly describes the electrons moving closer to the Na<sup>+</sup> during the POL process due to the

electrostatic attraction from Na<sup>+</sup>.

#### 4.6 $H_3O^+ - (H_2O)_5$ cluster

To demonstrate the capability of our polarization decomposition method to deal with clusters with more than two fragments, we show results for a  $\rm H_3O^+ - (H_2O)_5$  cluster, which is a simple model for solvated proton. We used the optimized structure from a previous publication <sup>71</sup> where the geometry is optimized at the  $\omega \rm B97X\text{-}V/def2\text{-}SVPD$  level. The EDA calculation was performed at the  $\omega \rm B97X\text{-}D/def2\text{-}TZVP$  evel.

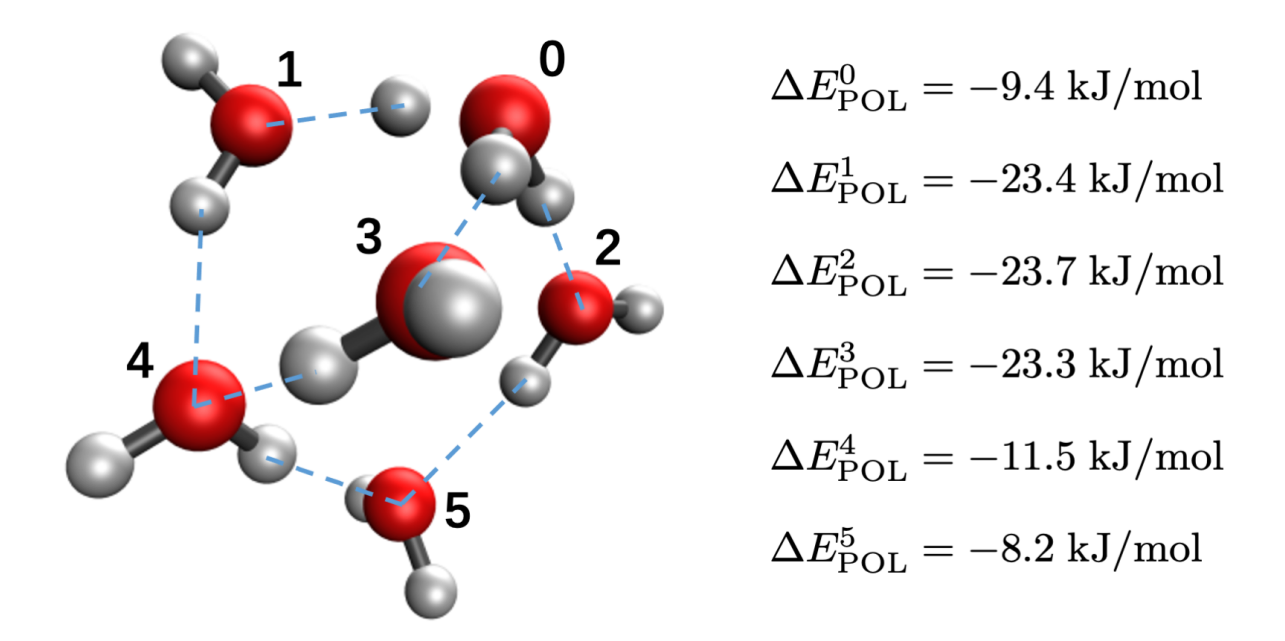


Figure 9: Structure of the  $H_3O^+-(H_2O)_5$  cluster with labels for each fragment (fragment 0 is the hydronium cation while the other 5 fragments are water molecules) and the polarization energy decomposed to each fragment. The blue dashed lines depicts the hydrogen bonding.

The  $H_3O^+ - (H_2O)_5$  cluster shown in Figure 9 is symmetric about the plane defined by the fragments 0, 4 and 5. Each of the water molecules 1, 2 and 3 is coordinated to a hydrogen atom of the hydronium cation to form a hydrogen bond. Together they form the so-called Eigen cation,  $H_3O^+(H_2O)_3$  which is the first solvation shell of the solvated hydronium cation. Water 4 forms two hydrogen bonds with water 1 and 3, while water 5 forms two hydrogen bonds with water 2 and 4, and they are part of the second solvation shell of the solvated hydronium cation. The polarization of the hydronium cation is largely due to the Pauli repulsion from the lone pairs of water molecules 1, 2 and 3, and its energy contribution is not very large since water molecules do not have permanent charge. The polarization energy of water molecules 1, 2 and 3 are roughly equal and quite large ( $\sim 24$  kJ/mol), since they are closest to the positively charged hydronium cation and have very similar chemical environments. Though both water molecules 4 and 5 are part of the second solvation shell, their contributions to the polarization energy are different and water molecule 4 polarizes more than water molecule 5. This is because water molecule 4 feels the induction from the solvated proton from two short paths 0-1-4 and 0-3-4, and one long path 0-2-5-4; while for the water molecule 5, the induction effect is transmitted from one short path 0-2-5 and two long paths 0-1-4-5 and 0-3-4-5. As induction decreases strongly with distance, it is reasonable that water molecule 5 should polarize less than water molecule 4.

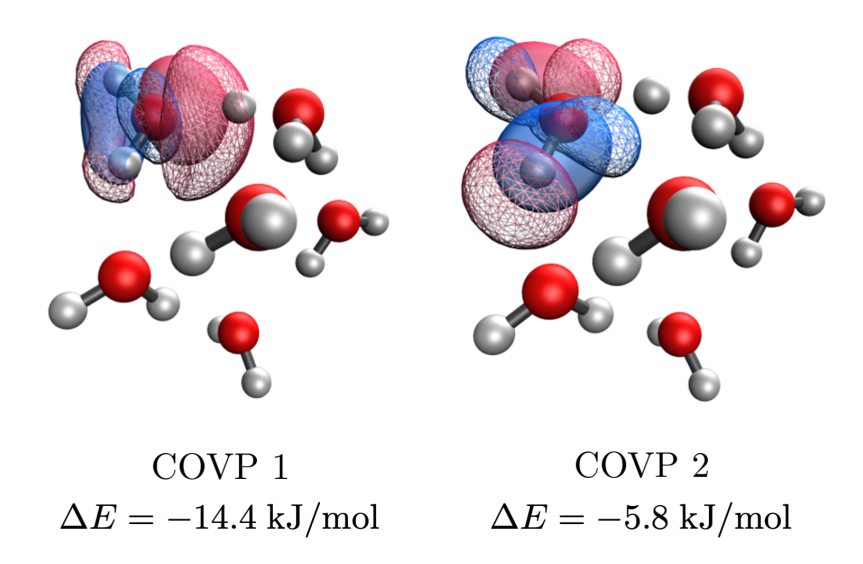


Figure 10: Two most significant COVPs for the polarization of water molecule 1.

Figure 10 shows the two most significant COVPs for the polarization of water molecule 1. It is clear that the most important COVP 1 describes the polarization of the oxygen lone pair while COVP 2 describes the polarization of the mixture of oxygen 2p orbital and hydrogen 1s orbitals of water. Remembering the significance of phase, we see that both of

these orbitals are polarizing towards the positively charged hydronium cation. The COVPs of other water molecules look similar to those of water molecule 1, with different directions depending on the direction of the hydrogen bond. This example shows how the POL analysis provides quantitative information about the chemical environment of each water molecule in a many-fragment complex.

#### 5 Conclusion

In this paper, we presented a non-perturbative energy decomposition analysis based on absolutely localized MOs (ALMOs) that can exactly unravel the energy decrease and charge rearrangements during the polarization (POL) process<sup>11</sup> into additive contributions from each molecule (or fragment) in a complex. The energy lowering,  $\Delta E_{POL}$ , is the energy change associated with on-fragment relaxation from isolated fragment orbital (the frozen state; <sup>44</sup> FRZ) subject to a fragment block-diagonal MO coefficient matrix via the SCF-MI procedure. <sup>18,21</sup> In order to ensure a polarized state with a valid complete basis set limit, fragment electric response functions (FERFs) <sup>11</sup> are used as the polarizing virtual orbitals of the frozen state for each fragment.

The computational cost of the polarization analysis is fairly small compared to the effort required to optimize the absolutely localized MOs (ALMOs) that define the polarized state. The additional work is associated with 3 additional Fock matrix constructions to perform the 5-point quadrature in Eq.30 (the end-points are already available), as well as some relatively inexpensive linear algebra steps that scale cubically with the size of each fragment. Therefore the POL analysis can be routinely performed as part of an ALMO-EDA calculation, similarly to the corresponding charge-transfer analysis.<sup>40</sup>

The resulting polarization analysis yields individual relaxation energies for each fragment that sum exactly to  $\Delta E_{\rm POL}$ . Given that polarization is well-understood to be a many-body process, <sup>42</sup> how is this possible? The answer is that our polarization analysis yields an exact

effective one-body picture of the true many-body (polarization) process. One way to see how this is possible is to consider a rearrangement of the many-body expansion (MBE):

$$E_{tot} = \sum_{i}^{N} E_{i} + \sum_{i < j}^{N} \Delta E_{ij} + \sum_{i < j < k}^{N} \Delta E_{ijk} + \sum_{i < j < k < l}^{N} \Delta E_{ijkl} + \cdots$$
 (54)

$$= \sum_{i}^{N} \left( E_i + \Delta E_i^{\text{eff}} \right) \tag{55}$$

This rearrangement can be viewed as a further condensation of the effective two-body interactions,  $^{43}$   $\Delta E_{ij}^{\text{eff}}$ . We are implicitly resumming many-body contributions (captured through SCF-MI) to allow us to evaluate the effective changes in 1-body energies due to polarization:

$$\Delta E_i^{\text{eff}} = \frac{1}{2} \sum_{j \neq i} \Delta E_{ij} + \frac{1}{3} \sum_{j < k \neq i} \Delta E_{ijk} + \frac{1}{4} \sum_{j < k < l \neq i} \Delta E_{ijkl} + \cdots$$
 (56)

$$= \frac{1}{2} \sum_{j \neq i} \Delta E_{ij}^{\text{eff}} \tag{57}$$

The one-body viewpoint is natural here because orbital relaxations corresponding to polarization occur on a single fragment. Other exact fragment-wise decompositions also exist.<sup>72</sup>

In addition, we implemented a complementary occupied virtual orbital pair (COVP) analysis that can further disentangle the energy decrease and charge transfer of the polarization process on a given fragment into contributions from important occupied-virtual pairs. In addition we established a very useful and general phase convention for COVPs. This phase convention allows intuitive connection between occupied and virtual orbital pairs: a region with constructive interference (same sign) corresponds to electron flow into that region, while regions with destructive interference (opposite sign) correspond to electron outflow.

A set of model examples, including the chloride water dimer, the water dimer, and one PAH complexes revealed interesting aspects of the polarization process that appear to be quite general. Specifically, we found that the polarization process cannot usually be compactly described by only one or two COVPs as in CT interactions. We presented examples where POL involves more than six COVPs with comparable contributions. These results demonstrate the polarization process as a complex and rather collective behavior of the electrons of each fragment in response to the fields and overlaps generated by other fragments. The most important COVPs typically correspond to the expected electrical induction, where electron pairs on one fragment are attracted to local sources of positive charge, or orient away from local sources of negative charge. We also found evidence for COVPs that correspond to relief of Pauli repulsions that may be present when forming a supersystem wavefunction from the frozen orbitals of the fragment. In repulsive regions of a potential energy surface these contributions can contribute to  $\Delta E_{\rm POL}$ . While we have concentrated on analyzing the distance dependence of the polarization contributions from entire fragments, it is also possible to examine the behavior of the individual COVPs as long as they can be followed. In principle, different COVPs could exhibit different decay behavior if they correspond to different mechanisms, such as electrical induction versus relief of Pauli repulsions.

In terms of limitations, the POL analysis reported here works well to provide insight into the relative contributions of each fragments to  $\Delta E_{\rm POL}$ , and the key polarizing orbitals. However, its success depends on the ability to separate a given complex into chemically meaningful fragments: this dependence on reference state is important to bear in mind for this analysis, as well as for EDA in general. As examples, the framework described here is not natural for intramolecular polarization, or for a system such as  $F^- \cdots H^+ \cdots F^-$  where the most appropriate fragments change with geometry.

# Conflicts of Interest

MH-G is a part-owner of Q-Chem Inc, whose software was used for all developments and calculations reported here.

# Acknowledgements

We would like to thank Alexander Zech for helpful discussions. This work was supported by the U.S. National Science Foundation through Grant No. CHE-1955643 and CHE-2313791, and additional support from CALSOLV.

# References

- (1) Bickelhaupt, F. M.; Baerends, E. J. Kohn-Sham Density Functional Theory: Predicting and Understanding Chemistry. *Rev. Comput. Chem.* **2000**, *15*, 1–86.
- (2) Hopffgarten, M.; Frenking, G. Energy Decomposition Analysis. Wiley Interdiscip. Rev.: Comput. Mol. Sci. 2012, 2, 43–62.
- (3) Phipps, M. J.; Fox, T.; Tautermann, C. S.; Skylaris, C.-K. Energy Decomposition Analysis Approaches and Their Evaluation on Prototypical Protein–Drug Interaction Patterns. Chem. Soc. Rev. 2015, 44, 3177–3211.
- (4) Andrés, J.; Ayers, P. W.; Boto, R. A.; Carbó-Dorca, R.; Chermette, H.; Cioslowski, J.; Contreras-García, J.; Cooper, D. L.; Frenking, G.; Gatti, C.; Heidar-Zadeh, F.; Joubert, L.; Pendás, A. M.; Matito, E.; Mayer, I.; Misquitta, A. J.; Mo, Y.; Pilmé, J.; Popelier, P. L. A.; Rahm, M.; Ramos-Cordoba, E.; Salvador, P.; Schwarz, W. H. E.; Shahbazian, S.; Silvi, B.; Solà, M.; Szalewicz, K.; Tognetti, V.; Weinhold, F.; Zins, E.-L. Nine Questions on Energy Decomposition Analysis. J. Comput. Chem. 2019, 40, 2248–2283.
- (5) Su, P.; Tang, Z.; Wu, W. Generalized Kohn-Sham Energy Decomposition Analysis and Its Applications. WIREs: Comput. Mol. Sci. 2020, e1460.
- (6) Mao, Y.; Loipersberger, M.; Horn, P. R.; Das, A.; Demerdash, O.; Levine, D. S.; Veccham, S. P.; Head-Gordon, T.; Head-Gordon, M. From Intermolecular Interaction Energies and Observable Shifts to Component Contributions and Back Again: A Tale of Variational Energy Decomposition Analysis. Annu. Rev. Phys. Chem. 2021, 72, 641–666.

- (7) Kitaura, K.; Morokuma, K. A New Energy Decomposition Scheme for Molecular Interactions within the Hartree-Fock Approximation. *Int. J. Quantum Chem.* **1976**, *10*, 325–340.
- (8) Khaliullin, R. Z.; Cobar, E. A.; Lochan, R. C.; Bell, A. T.; Head-Gordon, M. Unravelling the Origin of Intermolecular Interactions using Absolutely Localized Molecular Orbitals. J. Phys. Chem. A 2007, 111, 8753–8765.
- (9) Mitoraj, M. P.; Michalak, A.; Ziegler, T. A Combined Charge and Energy Decomposition Scheme for Bond Analysis. J. Chem. Theory Comput. 2008, 5, 962.
- (10) Su, P.; Li, H. Energy Decomposition Analysis of Covalent Bonds and Intermolecular Interactions. *J. Chem. Phys.* **2009**, *131*, 014102.
- (11) Horn, P. R.; Head-Gordon, M. Polarization Contributions to Intermolecular Interactions Revisited with Fragment Electric-Field Response Functions. J. Chem. Phys. **2015**, 143, 114111.
- (12) Mao, Y.; Ge, Q.; Horn, P. R.; Head-Gordon, M. On the Computational Characterization of Charge-Transfer Effects in Noncovalently Bound Molecular Complexes. J. Chem. Theory Comput. 2018, 14, 2401–2417.
- (13) Levine, D. S.; Head-Gordon, M. Energy Decomposition Analysis of Single Bonds within Kohn-Sham Density Functional Theory. *Proc. Natl. Acad. Sci. USA* **2017**, *114*, 12649.
- (14) Loipersberger, M.; Mao, Y.; Head-Gordon, M. Variational Forward–Backward Charge Transfer Analysis Based on Absolutely Localized Molecular Orbitals: Energetics and Molecular Properties. J. Chem. Theory Comput. 2020, 16, 1073–1089.
- (15) Jeziorski, B.; Moszynski, R.; Szalewicz, K. Perturbation Theory Approach to Intermolecular Potential Energy Surfaces of Van der Waals Complexes. *Chem. Rev.* **1994**, *94*, 1887.
- (16) Szalewicz, K. Symmetry-Adapted Perturbation Theory of Intermolecular Forces. Wiley Interdiscip. Rev.: Comput. Mol. Sci. 2012, 2, 254–272.
- (17) Patkowski, K. Recent Developments in Symmetry-Adapted Perturbation Theory. Wiley Interdiscip. Rev.: Comput. Mol. Sci. 2020, e1452.

- (18) Stoll, H.; Wagenblast, G.; Preuss, H. On the Use of Local Basis Sets for Localized Molecular Orbitals. *Theor. Chem. Acc.* **1980**, *57*, 169.
- (19) Gianinetti, E.; Raimondi, M.; Tornaghi, E. Modification of the Roothaan Equations to Exclude BSSE from Molecular Interaction Calculations. *Int. J. Quantum Chem.* **1996**, *60*, 157.
- (20) Nagata, T.; Takahashi, O.; Saito, K.; Iwata, S. Basis Set Superposition Error Free Self-Consistent Field Method for Molecular Interaction in Multi-Component Systems: Projection Operator Formalism. J. Chem. Phys. 2001, 115, 3553.
- (21) Khaliullin, R. Z.; Head-Gordon, M.; Bell, A. T. An Efficient Self-Consistent Field Method for Large Systems of Weakly Interacting Components. J. Chem. Phys. 2006, 124, 204105.
- (22) Horn, P. R.; Sundstrom, E. J.; Baker, T. A.; Head-Gordon, M. Unrestricted Absolutely Localized Molecular Orbitals for Energy Decomposition Analysis: Theory and Applications to Intermolecular Interactions Involving Radicals. J. Chem. Phys. 2013, 138, 134119.
- (23) Azar, R. J.; Horn, P. R.; Sundstrom, E. J.; Head-Gordon, M. Useful Lower Limits to Polarization Contributions to Intermolecular Interactions using A Minimal Basis of Localized Orthogonal Orbitals: Theory and Analysis of the Water Dimer. J. Chem. Phys. 2013, 138, 084102.
- (24) Lao, K. U.; Herbert, J. M. Energy Decomposition Analysis with A Stable Charge-Transfer Term for Interpreting Intermolecular Interactions. *J. Chem. Theory Comput.* **2016**, *12*, 2569.
- (25) Mo, Y.; Gao, J.; Peyerimhoff, S. D. Energy Decomposition Analysis of Intermolecular Interactions using A Block-Localized Wave Function Approach. J. Chem. Phys. 2000, 112, 5530–5538.
- (26) Mo, Y.; Song, L.; Lin, Y. Block-Localized Wavefunction (BLW) Method at the Density Functional Theory (DFT) Level. J. Phys. Chem. A 2007, 111, 8291–8301.
- (27) Mo, Y. R.; Bao, P.; Gao, J. L. Energy Decomposition Analysis Based on A Block-Localized Wavefunction and Multistate Density Functional Theory. Phys. Chem. Chem. Phys. 2011, 13, 6760-6775.

- (28) Horn, P. R.; Mao, Y.; Head-Gordon, M. Probing Non-Covalent Interactions with A Second Generation Energy Decomposition Analysis using Absolutely Localized Molecular Orbitals. *Phys. Chem. Chem. Phys.* 2016, 18, 23067–23079.
- (29) Mao, Y.; Levine, D. S.; Loipersberger, M.; Horn, P. R.; Head-Gordon, M. Probing Radical–Molecule Interactions with A Second Generation Energy Decomposition Analysis of DFT Calculations using Absolutely Localized Molecular Orbitals. Phys. Chem. Chem. Phys. 2020, 22, 12867–12885.
- (30) Morokuma, K. Why Do Molecules Interact? The Origin of Electron Donor-Acceptor Complexes, Hydrogen Bonding and Proton Affinity. *Acc. Chem. Res.* **1977**, *10*, 294–300.
- (31) Wu, Q.; Ayers, P. W.; Zhang, Y. Density-Based Energy Decomposition Analysis for Intermolecular Interactions with Variationally Determined Intermediate State Energies. J. Chem. Phys. 2009, 131, 164112.
- (32) Wu, Q. Variational Nature of the Frozen Density Energy in Density-Based Energy Decomposition Analysis and its Application to Torsional Potentials. *The Journal of Chemical Physics* **2014**, *140*, 244109.
- (33) Hayes, I.; Stone, A. An Intermolecular Perturbation Theory for the Region of Moderate Overlap. *Mol. Phys.* **1984**, *53*, 83–105.
- (34) Stone, A. J.; Misquitta, A. J. Charge-Transfer in Symmetry-Adapted Perturbation Theory. *Chem. Phys. Lett.* **2009**, 473, 201–205.
- (35) Misquitta, A. J. Charge Transfer from Regularized Symmetry-Adapted Perturbation Theory.

  J. Chem. Theory Comput. 2013, 9, 5313–5326.
- (36) Deng, S.; Wang, Q.; Ren, P. Estimating and Modeling Charge Transfer from the SAPT Induction Energy. J. Comput. Chem. 2017, 38, 2222–2231.
- (37) Glendening, E. D.; Feller, D. Cation-Water Interactions: The M+ (H2O) n Clusters for Alkali Metals, M= Li, Na, K, Rb, and Cs. J. Phys. Chem. 1995, 99, 3060.

- (38) Zhang, Y.; Wu, X.; Su, P.; Wu, W. Exploring the Nature of Electron-Pair Bonds: An Energy Decomposition Analysis perspective. *J. Phys. Condens. Matter* **2022**, *34*, 294004.
- (39) Khaliullin, R. Z.; Bell, A. T.; Head-Gordon, M. Analysis of Charge Transfer Effects in Molecular Complexes Based on Absolutely Localized Molecular Orbitals. J. Chem. Phys. 2008, 128, 184112.
- (40) Veccham, S. P.; Lee, J.; Mao, Y.; Horn, P. R.; Head-Gordon, M. A Non-Perturbative Pairwise-Additive Analysis of Charge Transfer Contributions to Intermolecular Interaction Energies. Phys. Chem. Chem. Phys. 2021, 23, 928–943.
- (41) Shen, H.; Wang, Z.; Head-Gordon, M. Generalization of ETS-NOCV and ALMO-COVP Energy Decomposition Analysis to Connect Any Two Electronic States and Comparative Assessment. J. Chem. Theory Comput. 2022, 18, 7428–7441.
- (42) Stone, A. The theory of intermolecular forces; Oxford University Press, 2013.
- (43) Mackie, C.; Zech, A.; Head-Gordon, M. Effective Two-Body Interactions. J. Phys. Chem. A 2021, 125, 7750–7758.
- (44) Horn, P. R.; Head-Gordon, M. Alternative Definitions of the Frozen Energy in Energy Decomposition Analysis of Density Functional Theory Calculations. J. Chem. Phys. 2016, 144, 084118.
- (45) Head-Gordon, M.; Maslen, P. E.; White, C. A. A Tensor Formulation of Many-Electron Theory in A Nonorthogonal Single-Particle Basis. *J. Chem. Phys.* **1998**, *108*, 616–625.
- (46) van Leeuwen, R.; Baerends, E. J. Energy Expressions in Density-Functional Theory using Line Integrals. *Phys. Rev. A* **1995**, *51*, 170.
- (47) Helgaker, T.; Jorgensen, P.; Olsen, J. Molecular electronic-structure theory; John Wiley & Sons, 2014.
- (48) Epifanovsky, E.; Gilbert, A. T.; Feng, X.; Lee, J.; Mao, Y.; Mardirossian, N.; Pokhilko, P.; White, A. F.; Coons, M. P.; Dempwolff, A. L., et al. Software for the frontiers of quantum

- chemistry: An overview of developments in the Q-Chem 5 package. *J. Chem. Phys.* **2021**, 155, 084801.
- (49) Chai, J.-D.; Head-Gordon, M. Long-Range Corrected Hybrid Density Functionals with Damped Atom-Atom Dispersion corrections. *Phys. Chem. Chem. Phys.* **2008**, *10*, 6615–6620.
- (50) Weigend, F.; Ahlrichs, R. Balanced Basis Sets of Split Valence, Triple Zeta Valence and Quadruple Zeta Valence Quality for H to Rn: Design and Assessment of Accuracy. Phys. Chem. Chem. Phys. 2005, 7, 3297.
- (51) Rappoport, D.; Furche, F. Property-Optimized Gaussian Basis Sets for Molecular Response Calculations. J. Chem. Phys. **2010**, 133, 134105.
- (52) Jr., T. H. D. Gaussian Basis Sets for use in Correlated Molecular Calculations. I. The Atoms Boron Through Neon and Hydrogen. J. Chem. Phys. 1989, 90, 1007.
- (53) Kendall, R. A.; Dunning Jr, T. H.; Harrison, R. J. Electron Affinities of the First-Row Atoms Revisited. Systematic Basis Sets and Wave functions. *J. Chem. Phys.* **1992**, *96*, 6796–6806.
- (54) Woon, D. E.; Dunning Jr, T. H. Gaussian Basis Sets for use in Correlated Molecular Calculations. V. Core-Valence Basis Sets for Boron Through Neon. J. Chem. Phys. 1995, 103, 4572–4585.
- (55) Hunter, J. D. Matplotlib: A 2D graphics environment. Comput. Sci. Eng. 2007, 9, 90–95.
- (56) Kandula, D. Z.; Gohle, C.; Pinkert, T. J.; Ubachs, W.; Eikema, K. S. Extreme Ultraviolet Frequency Comb Metrology. *Phys. Rev. Lett.* **2010**, *105*, 063001.
- (57) Lide, D. R. CRC handbook of chemistry and physics; CRC press, 2004; Vol. 85.
- (58) Weitzel, K.-M.; Mähnert, J.; Penno, M. ZEKE-PEPICO Investigations of Dissociation Energies in Ionic Reactions. *Chem. Phys. Lett.* **1994**, *224*, 371–380.
- (59) Joseph, J.; Jemmis, E. D. Red-, Blue-, or No-shift in Hydrogen Bonds: A Unified Explanation. J. Am. Chem. Soc. 2007, 129, 4620–4632.

- (60) Khaliullin, R. Z.; Bell, A. T.; Head-Gordon, M. Electron Donation in the Water-Water Hydrogen Bond. *Chem. Eur. J* **2009**, *15*, 851.
- (61) Ramos-Cordoba, E.; Lambrecht, D. S.; Head-Gordon, M. Charge-Transfer and the Hydrogen Bond: Spectroscopic and Structural Implications from Electronic Structure Calculations. Faraday Discuss. 2011, 150, 345.
- (62) Mao, Y.; Horn, P. R.; Head-Gordon, M. Energy Decomposition Analysis in An Adiabatic Picture. *Phys. Chem. Chem. Phys.* **2017**, *19*, 5944–5958.
- (63) Leger, A.; Puget, J. Identification of the 'Unidentified' IR Emission Features of Interstellar Dust? Astron. Astrophys. 1984, 137, L5–L8.
- (64) Allamandola, L.; Tielens, A.; Barker, J. Polycyclic Aromatic Hydrocarbons and the Unidentified Infrared Emission Bands-Auto Exhaust Along the Milky Way. Astrophys. J. 1985, 290, L25–L28.
- (65) Szczepanski, J.; Vala, M. Laboratory Evidence for Ionized Polycyclic Aromatic Hydrocarbons in the Interstellar Medium. *Nature* **1993**, *363*, 699–701.
- (66) Snow, T. P.; Le Page, V.; Keheyan, Y.; Bierbaum, V. M. The Interstellar Chemistry of PAH Cations. *Nature* **1998**, *391*, 259–260.
- (67) Szczepanski, J.; Banisaukas, J.; Vala, M.; Hirata, S.; Wiley, W. R. Preresonance Raman Spectrum of the C13H9 Fluorene-Like Radical. *J. Phys. Chem. A* **2002**, *106*, 6935–6940.
- (68) Zimmerman, P. M.; Musgrave, C. B.; Head-Gordon, M. A Correlated Electron View of Singlet Fission. Acc. Chem. Res. 2013, 46, 1339–1347.
- (69) Nakano, M. Open-Shell-Character-Based Molecular Design Principles: Applications to Non-linear Optics and Singlet Fission. *Chem. Rec.* **2017**, *17*, 27–62.
- (70) Baker, T. A.; Head-Gordon, M. Modeling the Charge Transfer between Alkali Metals and Polycyclic Aromatic Hydrocarbons using Electronic Structure Methods. J. Phys. Chem. A 2010, 114, 10326–10333.

- (71) Mackie, C. J.; Lu, W.; Liang, J.; Kostko, O.; Bandyopadhyay, B.; Gupta, I.; Ahmed, M.; Head-Gordon, M. Magic Numbers and Stabilities of Photoionized Water Clusters: Computational and Experimental Characterization of the Nanosolvated Hydronium Ion. The Journal of Physical Chemistry A 2023, 127, 5999–6011.
- (72) Altun, A.; Garcia-Ratés, M.; Neese, F.; Bistoni, G. Unveiling the Complex Pattern of Intermolecular Interactions Responsible for the Stability of the DNA Duplex. Chem. Sci. 2021, 12, 12785–12793.

# **TOC** Graphic

